Open access • Report • DOI:10.2172/188612

Design considerations on a proton superconducting linac — Source link

A.G. Ruggiero

Published on: 01 Aug 1995

Topics: Spallation Neutron Source, Particle accelerator, Linear particle accelerator and Neutron source

BNL 62312
Informal Report
Limited Distribution

Design Considerations on a Proton Superconducting Linac

Alessandro G. Ruggiero

August 1995

BNL Interdepartmental Study of a Spallation Neutron Source

Brookhaven National Laboratory
Upton, New York 11973

Work performed under the auspices of the U.S. Department of Energy

Disclaimer

BNL 62312
Informal Report
Limited Distribution

Design Considerations on a Proton Superconducting Linac*

Alessandro G. Ruggiero

August 1995

BNL Interdepartmental Study of a Spallation Neutron Source

Brookhaven National Laboratory
Upton, New York 11973

*Work performed under the auspices of the U.S. Department of Energy

Design Considerations on a Proton Superconducting Linac

Alessandro G. Ruggiero
Brookhaven National Laboratory
August 1995

Abstract

We analyze the longitudinal motion of a single proton in a superconducting linear accelerator. We derive the linearized equations of motion, and develop a matrix formalism to represent the progress of motion. The goal is to provide a tool which can be easily included in a computer code for the design of superconducting proton linacs. In particular we determine the stability conditions, and the amount of motion mismatch resulting from the presence of drift insertions, and from the rate of acceleration. Space-charge effects have not been included in the analysis. We complement the analysis with considerations of the rf and cryogenic power requirements, of the pulsed mode of operation, and of the beam transverse confinement. We conclude with an example of a Spallation Neutron Source.

1. Introduction

We consider a section of a superconducting linear accelerator for the acceleration of protons between the initial energy E_1 and the final energy E_2 which correspond to a velocity range, expressed in terms of the relativistic velocity factor, between β_1 and β_2.

We assume that the accelerator is a sequence of a number of identical *periods*, as shown in Figure 1. Each *period* is made of a cryo-module of length l_{cryo} and of an insertion of length l_{ins}. The insertion is needed for the placement of focussing quadrupoles, vacuum pumps, steering magnets, beam diagnostic devices, bellows and flanges. It can be either at room temperature or in a cryostat as well. The cryo-module includes M identical cavities each of N identical cells, and each having a length $L = Nl_c$, where l_c is the length of a cell. Cavities are separated from each other by a drift space d. An extra drift of length l_w may be added internally, on both sides of the cryo-module, to provide the transition between cold and warm regions. Thus,

$$l_{cryo} = M N l_c + (M - 1) d + 2 l_w \tag{1}$$

There are two symmetric intervals: a minor one, between the two middle-points A and B, as shown in Figure 1, which defines the interval of a cavity of length $L + d$; and a major one, between the two middle-points C and D, also shown in Figure 1, which defines the range of a *period* of total length $l_{cryo} + l_{ins}$. Thus the topology of a *period* can be represented as a drift of length g, followed by M cavity intervals, and a final drift of length g, where

$$g = l_w + (l_{ins} - d)/2 \tag{2}$$

Our goal is to determine the motion of a test particle in the longitudinal direction. After having

derived the equations of motion in the linear approximation, we shall develop a matrix method to describe the motion. For this purpose, we assume that all *periods* are identical, and that there is no energy change of the *reference* particle across a cryo-module. Acceleration is provided from one *period* to the next. The transfer-matrix method is very suitable for inclusion in a tracking or design computer code. Also, it allows estimation of the stability of the motion which may be disrupted by the insertion of drifts. Moreover, it is convenient for the estimation of motion mismatch in case the acceleration occurs at too large a rate.

At the end, we develop an operation model based on the assumption of constant energy gain per *period*. The choice of cryo-modules having all identical geometry and cavity/cell configuration is dictated by cost and construction handling. But there is, nevertheless, a penalty, in most cases of minor magnitude, due to the reduced transit-time-factors when crossing cavity cells, all with length adjusted to a common β value, which does not correspond to the particle's instantaneous velocity.

Longitudinal space-charge forces have not been included in the present analysis.

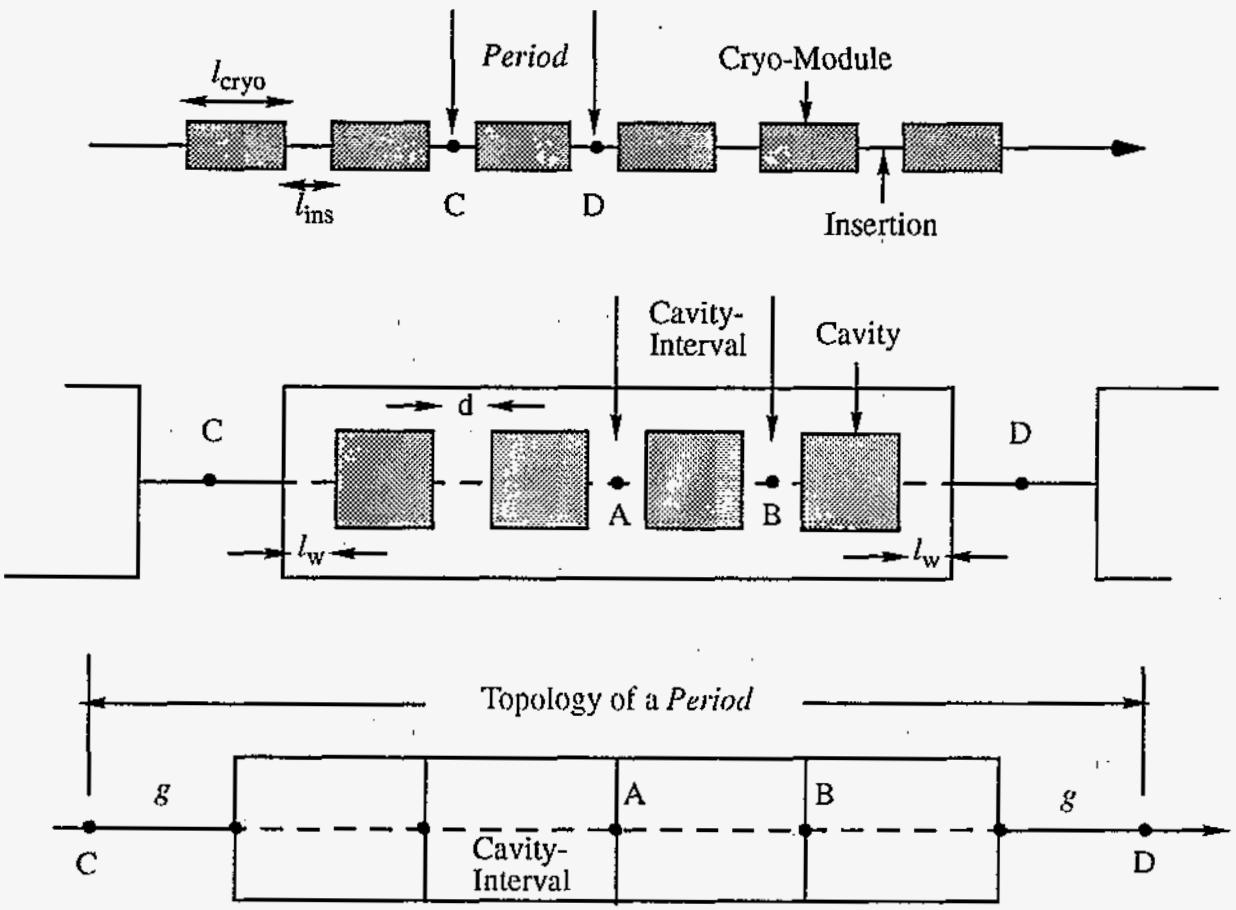

Figure 1. Configuration of a Proton Superconducting Linear Accelerator

2. The Linearized Equations of Motion

To describe the longitudinal motion of a single proton, let us take the canonically conjugated variables: the time delay τ and the energy difference ε with respect to the reference particle. We take also the longitudinal path length s as the independent variable. In the following a prime ($'$) will denote derivative with respect to s.

We have

$$\tau' = 1/v - 1/v_s , \tag{3}$$

where v is the velocity of the test particle, v_s that of the reference particle. After linearization,

$$\tau' = -\varepsilon / c\,\beta_s^3\,\gamma_s^3\,E_0 , \tag{4}$$

where c is the light velocity, E_0 is the proton energy at rest, and β_s, γ_s, respectively, the velocity and the energy relativistic factors of the reference particle.

If E is the total energy of the test particle, and E_s that of the reference particle,

$$\varepsilon = E - E_s . \tag{5}$$

The energy equations are

$$E' = e\,E_{acc}\ cos\,(\omega\,t) , \tag{6}$$

$$E_s' = e\,E_{acc}\ cos\,(\omega\,t_s) , \tag{7}$$

where e is the proton electric charge, E_{acc} the accelerating peak field, ω the angular frequency of the accelerating field, and t, t_s the traversal time-instants through the rf cavities, respectively, of the test and the reference particle, and

$$\tau = t - t_s . \tag{8}$$

Then

$$\varepsilon' = e\,E_{acc}\ [\,cos\,(\omega\,t) - cos\,(\omega\,t_s)\,] . \tag{9}$$

After linearization

$$\varepsilon' \doteq -e\,E_{acc}\ (\,sin\,\phi_s\,)\,\omega\,\tau , \tag{10}$$

where $\phi_s = \omega\,t_s$ is the synchronous rf phase angle.

Eq.s (4 and 10) are the linear equations of motion of the test particle. For a segment of the accelerating structure, short enough to neglect the variation of $\beta_s^3\,\gamma_s^3$, by combining the two equations,

we derive

$$\tau'' + K^2 \tau = 0, \tag{11}$$

with the restoring parameter

$$K = [\, e\, E_{acc}\, (-\sin \phi_s)\, \omega / c\, \beta_s^3\, \gamma_s^3\, E_0\,]^{1/2} = \Omega_s / c\, \beta_s, \tag{12}$$

and Ω_s is the longitudinal oscillation angular frequency.

3. Development of the Matrix Method

Let us now take τ and τ' as the variables that describe the motion of the test particle. τ' is related to the energy difference ε through Eq. (4). The status of motion can be represented by a column-vector of the two components τ and τ' to which we can apply a properly defined 2x2 transfer matrices. In a drift of length l, the transfer matrix is simply

$$M_{drift} = \begin{pmatrix} 1 & l \\ 0 & 1 \end{pmatrix}, \tag{13}$$

whereas in a rf cavity of length L

$$M_{cavity} = \begin{pmatrix} \cos\theta & (\sin\theta)\ /\ K \\ -K \sin\theta & \cos\theta \end{pmatrix}, \tag{14}$$

where the rotation angle $\theta = KL$.

Define the transfer matrix M_c between the two symmetry points A and B of a cavity-interval, as shown in Figure 1,

$$M_c = \begin{pmatrix} 1 & d/2 \\ 0 & 1 \end{pmatrix} \begin{pmatrix} M_{cavity} \end{pmatrix} \begin{pmatrix} 1 & d/2 \\ 0 & 1 \end{pmatrix}. \tag{15}$$

Because of symmetry, this matrix can be written as follows

$$M_c = \begin{pmatrix} \cos\mu_c & \beta_c \sin\mu_c \\ -(\sin\mu_c)/\beta_c & \cos\mu_c \end{pmatrix}, \tag{16}$$

where, denoting with η the ratio d / L,

$$K\beta_c = (\, 1 - \theta^2 \eta^2 / 4 + \theta \eta \cot\theta\,)^{1/2}, \tag{17}$$

$$L\, tg\, \mu_c = \quad \beta_c\, \theta \;/\; (\, cot\, \theta \;-\; \theta\, \eta\, /\, 2\,). \tag{18}$$

It is easy to derive the transfer matrix corresponding to the sequence of M identical cavity intervals. It is given by

$$M_c^{\,M} = \begin{pmatrix} cos\,(M\,\mu_c) & \beta_c\, sin\,(M\,\mu_c) \\ -\,[sin\,(M\,\mu_c)]\,/\,\beta_c & cos\,(M\,\mu_c) \end{pmatrix}. \tag{19}$$

We can also derive the total transfer matrix per *period* taken between middle-points C and D as shown in Figure 1.

$$M_c = \begin{pmatrix} 1 & g \\ 0 & 1 \end{pmatrix} \left(M_c^{\,M} \right) \begin{pmatrix} 1 & g \\ 0 & 1 \end{pmatrix}, \tag{20}$$

where g is given by Eq. (2). Because of symmetry, the transfer matrix per period has a form similar to Eq. (16), namely

$$M_p = \begin{pmatrix} cos\,\mu_p & \beta_p\, sin\,\mu_p \\ -\,(sin\,\mu_p)\,/\,\beta_p & cos\,\mu_p \end{pmatrix} = \begin{pmatrix} m_{11} & m_{12} \\ m_{21} & m_{22} \end{pmatrix}, \tag{21}$$

where

$$\beta_p = \{\, \beta_c^{\,2} - g^2 + 2\, g\, \beta_c\, cot\,(M\,\mu_c)\,\}^{\,1/2}, \tag{22}$$

$$tg\, \mu_p = \beta_p \;/\; [\, \beta_c\, cot\,(M\,\mu_c) \;-\; g\,]. \tag{23}$$

4. Beam Bunch Dimensions

The phase advance of the longitudinal oscillations is given by μ_c and μ_p, respectively, per cavity interval and per *period*. The amplitude function, which describes the beam bunch extension, has values β_c and β_p, respectively, between cavity intervals (middle-points A and B of Figure 1) and between *periods* (middle-points C and D of Figure 1).

Let $\Delta\tau$ be half of the bunch length in time units, and $\Delta\varepsilon$ be half of the energy spread. In those middle points with symmetry, the bunch ellipse in the phase plane (τ, ε) is upright; consequently the bunch area

$$S = \pi\, \Delta\tau\, \Delta\varepsilon \tag{24}$$

If the bunch area S is known, one can then estimate the bunch length from

$$\Delta\tau = (\, S\, \beta_{c,p} \,/\, \pi\, c\, \beta_s^{\,3}\, \gamma_s^{\,3}\, E_0\,)^{\,1/2} \tag{25}$$

Once the bunch length $\Delta\tau$ and area S are know, one derives the energy spread $\Delta\varepsilon$ from Eq. (24).

5. Stability of Motion

For the motion to be stable across a cavity interval or across a *period*, the values of the amplitude function given by Eq.s (17 and 22) must satisfy the relation

$$\beta_{c,p} > 0 \tag{26}$$

The value β_c is plotted in Figure 2 versus the rotation angle θ for several values of the ratio η. In the limit $d = 0$, $\beta_c = 1/K$, and the motion is always stable. As the length of the insertion increases, with respect to the cavity length L, the permissible range of values of the rotation angle, that is of the accelerating gradient, reduces. The limit of stability, which is the maximum permissible value of θ, is given in Figure 3 where it is plotted versus the ratio η.

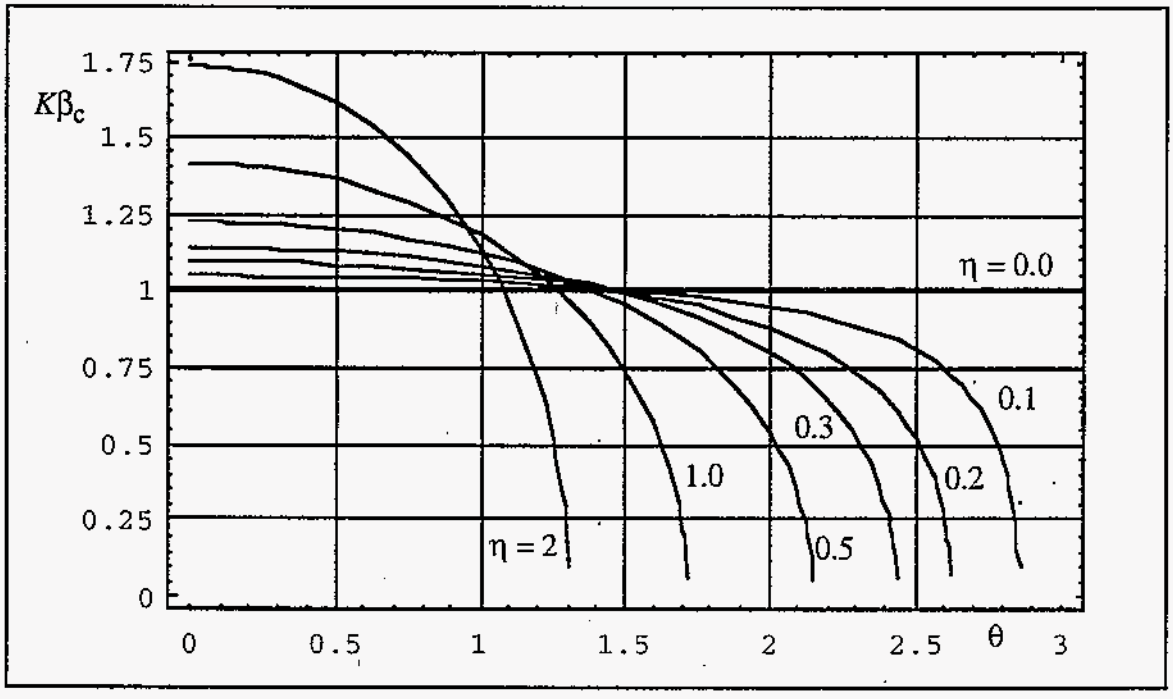

Figure 2. Plot of $K\beta_c$ versus the rotation angle θ, for several values of the ratio $\eta = d/L$.

Similarly, the amplitude value β_p is plotted in Figure 4 versus the phase advance $M\mu_c$ corresponding to M cavities, for several values of the ratio g / β_c. It is seen that in the limit $g = 0$, $\beta_p = \beta_c$, and the motion is everywhere stable.

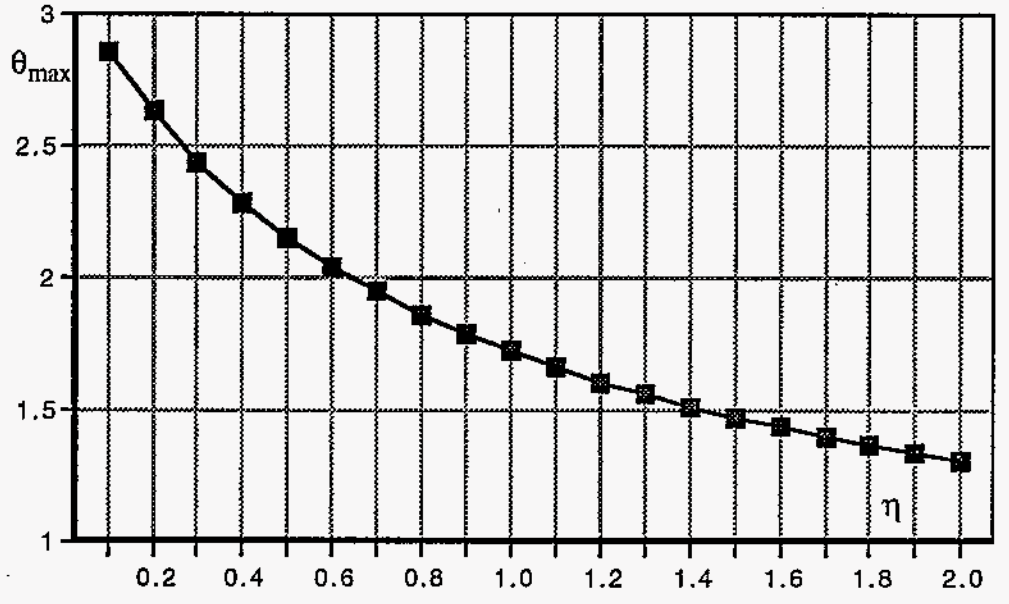

Figure 3. Plot of the rotation angle θ at the limit of stability versus the ratio $\eta = d/L$.

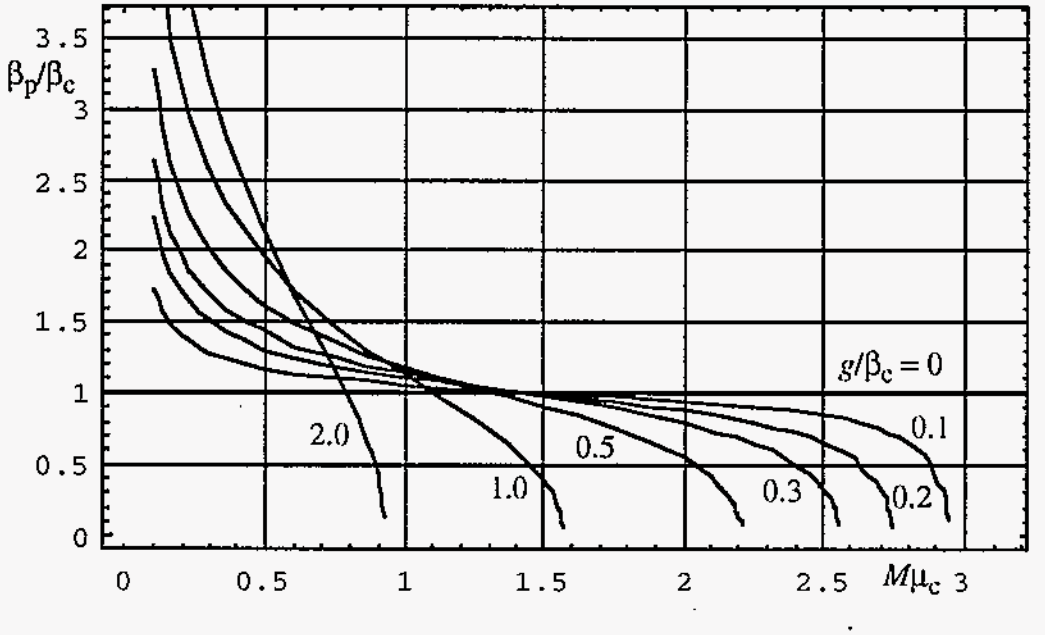

Figure 4. Plot of the ratio β_p / β_c versus $M\mu_c$, for several values of the ratio g / β_c .

8. Mismatch of Motion

We have assumed that the restoring parameter K does not change across the length of a *period*. This assumption is justified when indeed the acceleration rate is not too high, and the energy change of the reference particle is small compared to the total kinetic energy.

Complete matching of the motion as it progresses down the length of the linear accelerator is achieved by requiring that the amplitude value β_p remains constant from a period to another. From Eq. (22) we infer that this requires that in turn also β_c and the phase advance μ_c per cavity-interval remain also unchanged. That is, from Eq.s (17 and 18), that the rotation angle θ, and thus the restoring parameter K are also constant. For a constant accelerating frequency ω, and constant rf phase angle ϕ_s, we derive the following condition for complete matching

$$E_{acc} \; / \; \beta_s^{\,3} \gamma_s^{\,3} \;\; = \;\; \text{constant} \qquad (27)$$

which assigns how the accelerating field E_{acc} has to vary with the beam energy.

This condition is usually difficult to meet in practice. Thus a different, simpler mode of operation is proposed which assumes a constant energy gain per *period*, that is per cryo-module. Since all the cryo-modules are identical, with the same geometry, number of cavities and cells per cavity, this mode of operation leads to the same energy gain also per cavity and per cell everywhere. If we denote with U the energy gain per cell, the energy gain per cavity is MU and that per *period* is MNU. From Eq. (7)

$$U \;\; = \;\; \quad e\, l_c\, E_{acc}\, cos\, \phi_s \,. \qquad (28)$$

The constant energy-gain mode of operation yields to a constant accelerating field E_{acc}, so that the value of the restoring parameter K will vary and decrease with the beam energy. This will cause a continuous mismatch of the particle motion, that is a beam bunch dilution of an amount which depends on the acceleration rate, and on the length of the drift insertions. In analogy to the conventional approach used to describe the transverse motion, a beam bunch can be made to correspond to an ellipse in the phase space (τ, τ'). Between *periods*, the ellipse is described by the local amplitude function β_p and the inclination function α_p. To estimate the amount of mismatch as the motion progress, we assume that the dimensions of the beam bunch are exactly matched at the entrance of the linac section, where $\alpha_p = 0$ and β_p is given by Eq.(22). It is well known then how to estimate the bunch ellipse rotation, dilation or contraction from one *period* to the next. This will yield an amplitude functions which in general will be different from β_p, and an inclination function with values oscillating around zero. The propagation of the ellipse orientation and elongation/dilation across one *period* (from midpoint "1" to midpoint "2") is given by

$$\begin{pmatrix} \beta_p \\ \alpha_p \\ \gamma_p \end{pmatrix}_2 \;\; = \;\; \begin{pmatrix} m_{11}^{\,2} & -2\, m_{11} m_{12} & m_{12}^{\,2} \\ -m_{21} m_{11} & 1 + 2\, m_{12}\, m_{21} & -m_{12} m_{22} \\ m_{21}^{\,2} & -2\, m_{22}\, m_{21} & m_{22}^{\,2} \end{pmatrix} \;\; \begin{pmatrix} \beta_p \\ \alpha_p \\ \gamma_p \end{pmatrix}_1 \qquad (29)$$

where $\beta_p \gamma_p = 1 + \alpha_p^{\,2}$, and the elements m_{ij} are given in Eq. (21).

9. RF Power Considerations

The total rf power required to operate one cryo-module is the sum of three contributions:

$$P_{rf} = P_b + P_w + P_{HOM} \tag{30}$$

where the beam power, denoting with I_b the beam current,

$$P_b = MNU\, I_b / e\,. \tag{31}$$

P_w is the wall-dissipated power, and P_{HOM} the power dissipated to the cavity high-order resonating modes. In a superconducting linac for protons, one expects $P_w + P_{HOM} << P_b$, so that the rf power requirement is dominated by the beam power. Denoting with P_{coup} the rf power in each of the rf couplers driving the cavity system, and by n_{coup} the number of couplers per cryo-module

$$P_{coup} \sim P_b / n_{coup}\,. \tag{32}$$

This amount is constant and the same from one *period* to the next.

The energy gain per cell U is given by Eq.(28) and depends on the accelerating field E_{acc}. This in turn depends on the transit-time factor $T(\beta)$ which is a function of the cell geometry, and of the beam velocity β. Since all the cavity cells in the linac structure have been adjusted to the same length l_c, denoting with E_0 the actual axial field in a given cell,

$$E_{acc} = E_a\ T(\beta) / T(\beta_0) \tag{33}$$

where

$$E_a = E_0\, T(\beta_0) \tag{34}$$

For half-wavelength cavity-cells the optimum cell length should be adjusted to

$$l_c = \lambda\, \beta_0 / 2 \tag{34}$$

where λ is the accelerating field wavelength. Otherwise the transit-time factor

$$T(\beta) = H(a)\, F_N(\beta, \beta_0)\, sin\,(\pi\, l_c / \beta\, \lambda\,) / (\pi\, l_c / \beta\, \lambda\,) \tag{35}$$

where

$$F_N(\beta, \beta_0) = (-1)^{(N-1)/2}\, cos\,(N \pi\, \beta_0 / 2\, \beta\,) / N\, cos\,(\pi\, \beta_0 / 2\, \beta\,) \quad \text{for } N, \text{ odd} \tag{36}$$

$$= (-1)^{N/2+1}\, sin\,(N \pi\, \beta_0 / 2\, \beta\,) / N\, cos\,(\pi\, \beta_0 / 2\, \beta\,) \quad \text{for } N, \text{ even} \tag{37}$$

is a form factor which gives the energy gain of a proton with velocity β traversing a cavity made of N cells of length given by Eq. (34). These form factors are unit for $\beta = \beta_0$. Finally,

$$H(a) = 1 / I_0 (2 \pi a / \beta_0 \gamma_0 \lambda) \quad (38)$$

is a cavity-aperture factor for radial aperture a, and I_0 is the modified Bessel function. For an assigned amount of rf power in the couplers, as the beam velocity varies from a *period* to the next, the transit-time factor $T(\beta)$ will vary also, and the axial field E_0 will then be adjusted accordingly so that E_{acc} is constant with a value given by combining Eq.s (28, 31,33 and 34).

The power dissipated on the cavity walls per cryo-module is

$$P_w = NM l_c E_0^2 / R_s = NM l_c E_a^2 / Z_0 T_0^2 Q_0 \quad (39)$$

where $T_0 = T(\beta_0)$, $R_s = Z_0 Q_0$ is the shunt impedance per unit of length, Z_0 is the cavity characteristic impedance, also per unit of length, and Q_0 the unloaded figure of merit. Depending on the choice of the cell length l_c and of the reference value β_0, typical values of $Z_0 T_0^2$ are in the range of few hundred ohm/m. The figure of merit Q_0 can be estimated from the formula

$$Q_0 = 10^9 G / R_w \quad (40)$$

where G is a cell geometry factor of a value around 250 β_0, and R_w is the surface impedance, given in nohm,

$$R_w = R_{res} + (0.1 \text{ nohm }) f_{rf}^2 \, exp(-18/T_k) / T_k, \quad (41)$$

where R_{res} is the residual impedance with a value of about 20 nohm, T_k is the environment temperature in degrees Kelvin, and f_{rf} is the rf frequency in MHz.

The power dissipated to the high-order modes of the cavity in one cryo-module can be estimated from the equation

$$P_{HOM} = (1.7 \times 10^{-6} \text{ Watt }) NM f_{rf} I_b^2, \quad (42)$$

where f_{rf} is in MHz and the average beam current I_b in mA.

Note that, whereas the power P_{HOM} dissipated to the high-order modes is constant, the wall-dissipated power P_W varies from *period* to *period*.

The AC power requirements to operate the complete rf system depends on the RF-to-AC efficiency

$$P_{AC} = P_{rf} / \eta_{rf}, \quad (43)$$

where P_{rf} is given by Eq. (30). For high-power Klystrons typically $\eta_{rf} \sim 0.585$, and for lower-power Klystrodes $\eta_{rf} \sim 0.7$. These figures include dissipation in the rf waveguides (~ 5%) and DC-to-AC conversion efficiency (~ 99%).

10. Cryogenic Power Considerations

The total cryogenic power per cryo-module that is required in a superconducting linac for protons is made of three contributions

$$P_{cryo} = \quad P_w + P_{HOM} + P_s, \tag{44}$$

where the power P_w dissipated on the cavity walls and the power P_{HOM} dissipated to the high-order modes are already given, respectively, by Eq.s (39 and 42). The last contribution P_s is the static loss which is dissipated through the walls of the cryostat

$$P_s \quad = \quad W_{cryo}\, l_{cryo}, \tag{45}$$

where typically $W_{cryo} = 5$ W/m.

The AC power requirement depends on the conversion efficiency which, unfortunately, for cryogenic systems is quite low. It depends also on the final required temperature.

$$P_{AC} \quad = \quad P_{cryo} / \eta_{cryo}. \tag{46}$$

For an environment around 4.2 °K, one can expect $\eta_{cryo} \sim 0.004$.

11. Pulsed Superconducting Linacs

For the continuous mode of operation of a superconducting linac for protons, average and peak values are equal. This is not so for a pulsed mode of operation. In this case one defines a repetition rate f_{rep}, a pulse length T_p, and a duty cycle

$$\delta \quad = \quad T_p\, f_{rep}, \tag{47}$$

which is the fraction of the total time when beam is present and accelerated. In this case, average and peak values, like beam current, rf power and so on, differ from each other. If all the accelerator and beam parameters defined above refer to peak values, the corresponding average values can be denoted within brackets, and in principle can be simply derived after multiplying the peak values with the duty cycle. There is one difference, that is, just before the beam is injected into the linac for acceleration, the rf cavities are to be refilled with rf energy. This takes an amount of time T_F which has the effect of lengthening the duty cycle so that the total running time is $T_p + T_F$. Since the beam is present only during the period of length T_p, the average values are

$$\langle I_b \rangle \quad = \quad \delta\, q\, I_b \tag{48}$$

$$\langle P_{rf} \rangle \quad = \quad \delta\, (q\, P_b + P_w)\, (1 + T_F / T_p) + \delta\, q\, P_{HOM} \tag{49}$$

$$\langle P_{cryo} \rangle \quad = \quad \delta\, P_w\, (1 + T_F / T_p) + \delta\, q\, P_{HOM} + P_s \tag{50}$$

In Eq.(48), I_b actually denotes the proton beam peak current, and q (~ 60%) is a chopping ratio, typically at frequencies around the MHz value, as it may be in the case when the beam is to be injected in a ring. The filling time T_F is given by

$$T_F = 1.4 (Q_0 / \omega) / (2 + P_b / P_w) \quad (51)$$

Pulsing a superconducting linac has of course several technical implications. The rf pulsing is performed by modulators or circulators, which are electronic components with difficulties that depend on the choice of frequency, pulse duration, repetition rate, and the excursion of rf power. Moreover, Klystrons may be significantly less efficient (η_{rf} ~ 0.45), since the cathode voltage has to be lowered. Finally, there are problems associated with frequency detuning caused by the Lorentz forces and microphonics. In principle, though, all these problems can be tackled and resolved.

12. Transverse Beam Confinement

The transverse motion of protons is confined with quadrupole magnets located in the insertions between cryo-modules. There are two possible arrangements: FODO and doublets. The first has a single quadrupole per insertion with alternating polarity from one insertion to the next. The second arrangement is made of a sequence of pairs of quadrupoles (doublets), of opposite polarity, per insertion. The gradient B' of quadrupoles varies with the beam energy, that is the magnetic rigidity $B\rho$, so that the focussing parameter $k = B' / B\rho$ is constant. This will ensure continuous matching of the transverse motion.

Denoting with ε_n the normalized betatron emittance of the beam (for instance, the rms value), the rms beam radius at a quadrupole location where the amplitude function has the largest value β_Q is

$$b = (\varepsilon_n \beta_Q / \pi \beta\gamma)^{1/2}. \quad (52)$$

Denoting with ψ the betatron phase advance per *period* of length $L_p = l_{cryo} + l_{ins}$, in the case of the FODO arrangement, using the thin-lens approximation,

$$\beta_Q = (L_p / \sin \psi) [(1 + \sin \psi) / (1 - \sin \psi)]^{1/2}, \quad (53)$$

$$k l_Q = (2 \sin \psi) / L_p . \quad (54)$$

where l_Q is the quadrupole length. Whereas for the doublet arrangement,

$$\beta_Q = \{ L_p + 2 [d_Q (L_p - d_Q)]^{1/2} \sin (\psi/2) \} / \sin \psi, \quad (53)$$

$$k l_Q = 2 \sin (\psi/2) / [d_Q (L_p - d_Q)]^{1/2}. \quad (54)$$

where d_Q is the space between the quadrupoles of the same doublet. If a denotes the inner radius of the cavities, assuming it is equal to that of the vacuum chamber in the insertions and elsewhere, one desires that the ratio a / b is maintained at a large value (> 20) to avoid latent activation

effects that may be caused by uncontrolled beam losses. The FODO arrangement takes less space, and requires less field gradient, but the doublet arrangement would give the smallest beam size overall.

13. General guidance for the cost estimate of a superconducting linac

In order to make comparisons of different linac designs, and to allow analysis of trading between cost and performance, it is useful, at the design stage, to have some guidance on the estimating of the cost of a superconducting linac. The following are simple parametric estimates which are to be taken with caution; they provide only an indication of the behavior of the overall cost, and should be followed by a more-detailed engineering cost estimate, once all the accelerator components have been identified.

There are two contributions to the overall cost: Capital (direct) Cost needed for the construction proper of the accelerator, and Operation Cost. The Capital Cost can be broken down in the following major components:

Insertion (assuming normal conducting) including vacuum chamber with flanges and bellows, quadrupole magnets, steering dipoles and beam position monitors vacuum port, and vacuum pump	100 k$ /m
Superconducting structure including cryostats with feed-throughs, internal refrigeration rf cavities and vacuum chamber	300 k$ /m
Tunnel, with service buildings	70 k$ /m
Refrigeration Plant with piping	2 k$/ W @ 4.2 ^{o}K
Electrical Distribution	0.14 $/ W of AC power
RF Power, including Klystrons (assuming 2 Cavities per Klystron) rf Couplers, waveguides, rf windows (assuming 1 rf Coupler per Cavity) Power distribution	
CW-Mode	1.68 $/ W of rf power
Pulsed-Mode	2.50 $/ W of rf power

The Operation Cost depends on the availability (75 %) required over one-year period of the accelerator, and is eventually given as the cost for one-year operation as well as the cumulative cost over a longer period of time (~ 10 years). Most of the cost is the electricity bill which can be

estimated as 0.05 $/kWh of total AC power, which is an average of the electricity cost across the United States. We are not including here cost for maintenance, replacement material, and labor for operation.

The linear accelerator can also be rated with an efficiency parameter: the ratio of average the beam power to the total required AC power.

14. An Example of Spallation Neutron Source

The following is an example of a 2.4-GeV superconducting linac which can be used as a Spallation Neutron Source. One can conceive three modes of operation, shown also in Figure 5:

> Continuous Wave (CW) of protons with the average beam power of 60 MW and an average accelerated beam current of 25 mA. A continuous positive-ion source of 30 mA is required for this mode of operation. No beam chopping is needed.
>
> Long Pulses (LP) of protons in the millisecond range. The linac is operated at either 10 or 60 pulses per second with a duty cycle of 1 to 10%. A 30-mA positive-ion source is still required which can be pulsed accordingly, but no beam chopping is needed. The average beam power ranges between 1 and 6 MW depending on the pulse length and on the repetition rate. The linac needs to be pulsed.
>
> Short Pulses (SP) of microsecond duration of protons. This can be obtained only by injecting the beam, in many turns, in one Compressor Ring, with a negative-ion source, and the charge-exchange injection method, for a more efficient transfer of the beam into the Ring. Moreover, the beam will have to be pre-chopped by about 60%. Expected average beam power will range between 1 and 5 MW, depending on the linac pulse length and on repetition rate.

The Linac itself is made of four sections. The first section includes the ion source, two RFQs for acceleration to 5 MeV, and a conventional, normal-conducting Drift Tube Linac for acceleration to 100 MeV. The front-end section operates at the frequency of 350 MHz, and the DTL at 700 MHz, to allow funneling of two ion beams, if it is required in the future. The superconducting linac is made of the three following sections, all operating at 700 MHz. The first section accelerates from 100 to 300 MeV, the second from 0.3 to 1.2 GeV, and the last section from 1.2 to 2.4 GeV. The division in sections allows ranges of beam velocity β sufficiently narrow that one can operate them with constant cryo-module configuration without too much loss of accelerating gradient, because of the reduced transit-time factors. In each of the three superconducting sections the cavity-cell length l_c is adjusted to yield the optimum transit-time factor at an intermediate β value. The major parameters of the superconducting Linac are shown in Table 1, and those for each of the three sections in Table 2. The cavity filling times T_F are shown in Figure 15.

For the Long-Pulse mode of operation, the average available beam power and the average required rf power can be expressed as functions of the beam pulse length T_P and the repetition rate f_{rep}. The summary is given in Figures 16 and 17, where the required average total AC power

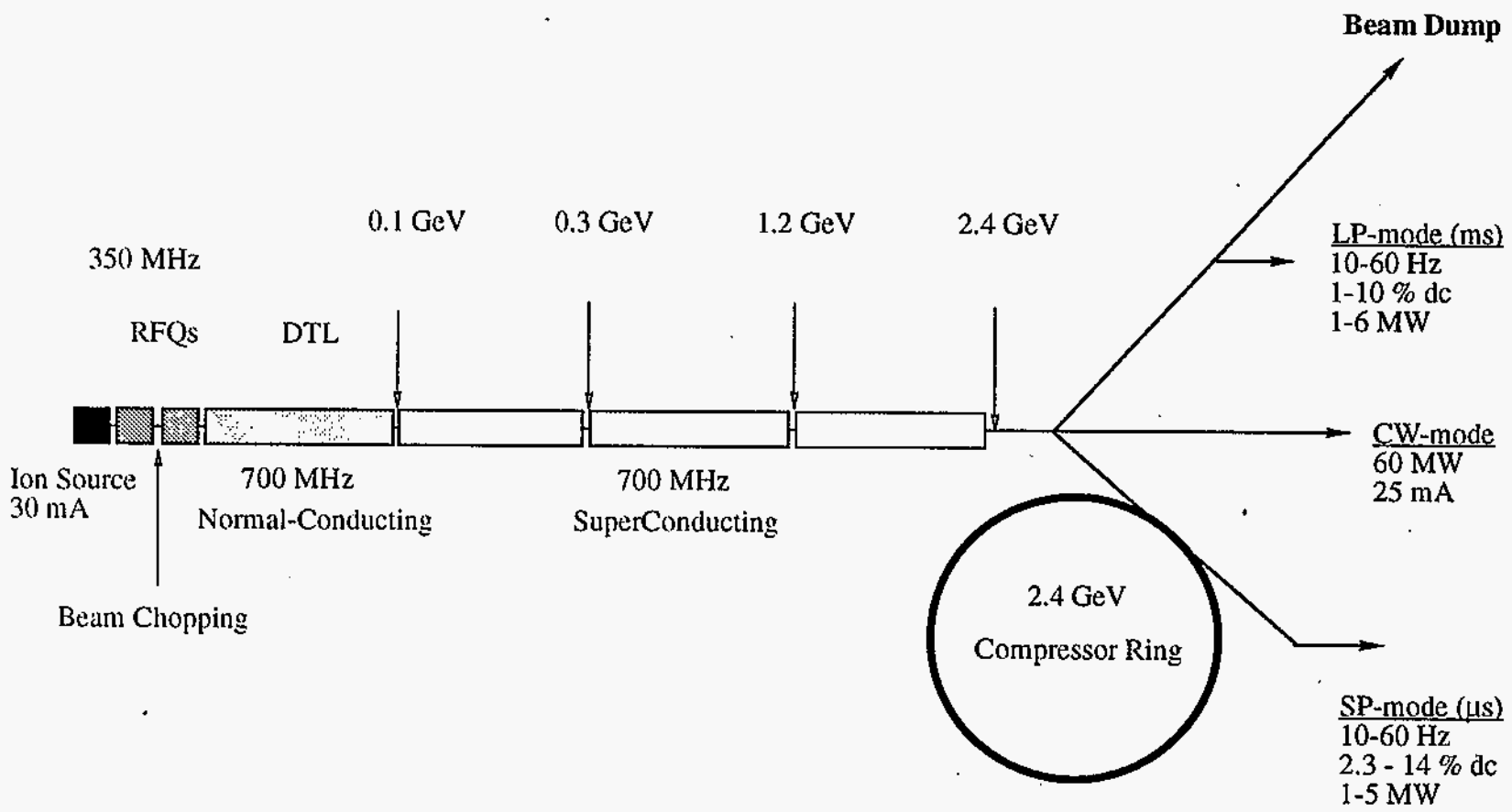

Figure 5. Layout of the Spallation Neutron Source using a 2.4 GeV Superconducting proton Linac

Table 1. General Parameters of the 2.4-GeV Superconducting Linac

Total Beam Power (CW)	60 MW
Beam Current, I_b	25 mA
Ion Source Current	30 mA
Initial Kinetic Energy	100 MeV
Final Kinetic Energy	2.4 GeV
Frequency	700 MHz
No. of Protons / Bunch	4.5×10^8
Temperature	4.2 °K
Cells / Cavity, N	4
Cavity Separation, d	32 cm
Cold-Warm Transition, l_w	30 cm
Accelerating Gradient, E_a	7.302 MeV/m
Cavities / Klystron	2
No. of rf Couplers / Cavity, n_{coup}	1
RF Phase Angle	-30°
Method for Transverse Focussing	FODO
Betatron Phase Advance / FODO cell	90°
Normalized rms Emittance	0.29 π mm mrad
rms Bunch Area	1.917 π eV-s

is also shown, together to the capital and operation cost, versus the beam pulse length.

Beam pulses of shorter lengths, around a microsecond, can be obtained only with a negative-ion source and by accumulating several beam turns in one Accumulator Ring, where the beam can be compressed to the required length. For this mode of operation, the beam is to be chopped at a ratio $q = 60\%$, at the revolution frequency of the Accumulator Ring. Moreover, the Linac is to be pulsed at a repetition rate which is either 10 or 60 Hz. Assuming a beam peak power of 60 MW, an average beam power of 5 MW at the repetition rate of 60 Hz, with a chopping ratio of 60%, requires a pulse length of 2.315 ms. Taking a maximum of 1000 beam turns injected into the Accumulator Ring, one derives 666 m for the circumference of the Ring. The summary of parameters for the Short-Pulse mode of operation is given in Table 3.

Acknowledgments

The Author wishes to thank Dominic Chan, and Tom Wangler, of Los Alamos National Laboratory, for the opportunity given to him of doing this work. He also thanks them and Klaus Bongardt of Julich, Germany, for useful discussions on several technical issues described in this report.

Table 2. Summary of the 2.4-GeV 25-mA Superconducting Linac Design

		Low-Energy	Medium-Energy	High-Energy
Energy: in		100 MeV	300 MeV	1.2 GeV
out		300 MeV	1.2 GeV	2.4 GeV
Velocity, β: in		0.4282	0.6526	0.8986
out		0.6526	0.8986	0.9597
Cell Reference β_0		**0.48**	**0.71**	**0.93**
Cell Length, l_c cm		10.28	15.20	19.91
Total No. of *Periods*		13	59	60
Cavities / Cryo-Module, M		6	4	4
Length of Insertion, l_{ins} m		1.079	1.753	1.753
Length of a Period, L_p m		5.746	5.746	6.499
β_Q, m		19.6	19.6	22.2
Total Length, m		**74.70**	**338.99**	**389.96**
Coupler rf Power, kW		65.0	96.2	125.9
Energy Gain/Period, MeV		15.60	15.38	20.15
Total No. of Klystrons		39	118	120
Klystron Power, kW (*)		175	260	340
$Z_0T_0^2$, ohm/m		223	488	837
Q_0		0.66×10^9	0.97×10^9	1.27×10^9
Dissipated Power, kW		13.80	17.17	9.52
HOM-Power, kW		0.234	0.708	0.720
Cryogenic Power, kW		14.33	19.05	11.66
Beam Power, MW		5.00	22.50	30.00
Total rf Power, MW		5.01	22.52	30.01
AC Power for rf, MW		8.57	38.49	51.30
AC Power for Cryo., MW		3.58	4.76	2.92
Total AC Power, MW		**12.15**	**43.26**	**54.22**
Efficiency, %		**41.1**	**52.0**	**55.3**
Capital Cost:	rf Klystrons	8.424	37.83	50.417
	Electr. Distr.	1.702	6.056	7.590
	Refrig. Plant	28.667	38.106	23.326
	Warm Struct.	1.403	10.343	10.518
	Cold Struct.	18.201	70.669	85.435
	Tunnel	5.229	23.729	27.297
Total Cost, M$		**63.625**	**186.733**	**204.584**
Operation Cost, M$/y		**3.993**	**14.209**	**17.810**

(*) Including 35% power contingency

Table 3. Short-Pulse Mode of Operation

Repetition Rate, Hz	10		60
Pulse Length, ms		2.315	
Chopping Ratio, %		60	
Chopping Frequency, MHz		0.432	
Duty Cycle, %	2.315		13.89
Number of Beam Turns injected		1000	
Accumulator Ring Circumference, m		666	
Peak Beam Current, mA		25	
Average Beam Current, mA	0.579		3.473
Average Beam Power, MW	0.833		5.0
Average rf Power, MW	0.87		5.23
Average Cryogenic Power, kW	3.48		6.34
Average total AC Power, MW	2.80		13.21
Efficiency, %	29.75		37.85
Capital Cost, M$	262.350		280.425
Operation Cost, M$/year	0.921		4.338

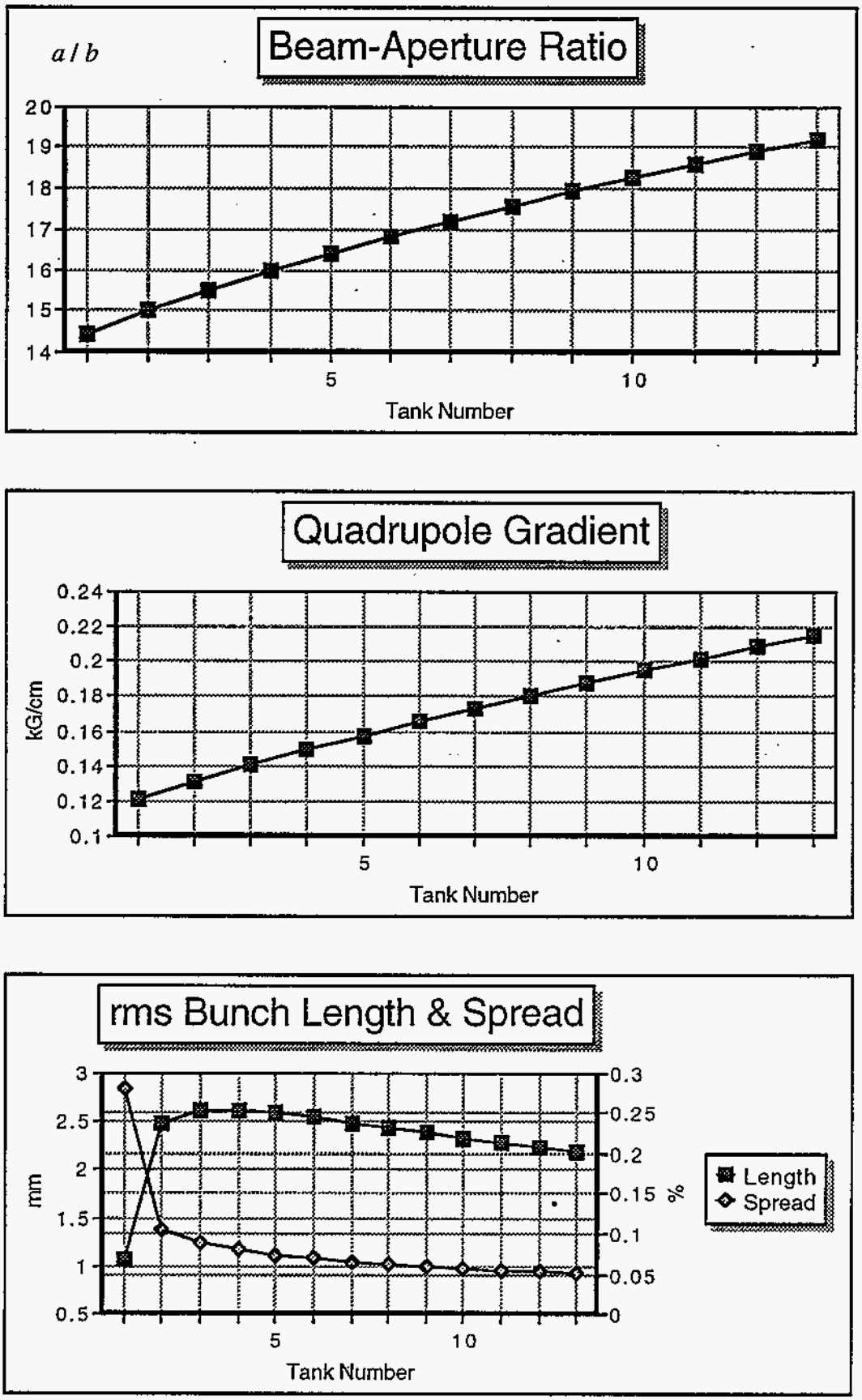

Figure 6. Plots (1) of Behavior versus *period* (tank) number of the Low-Energy Section

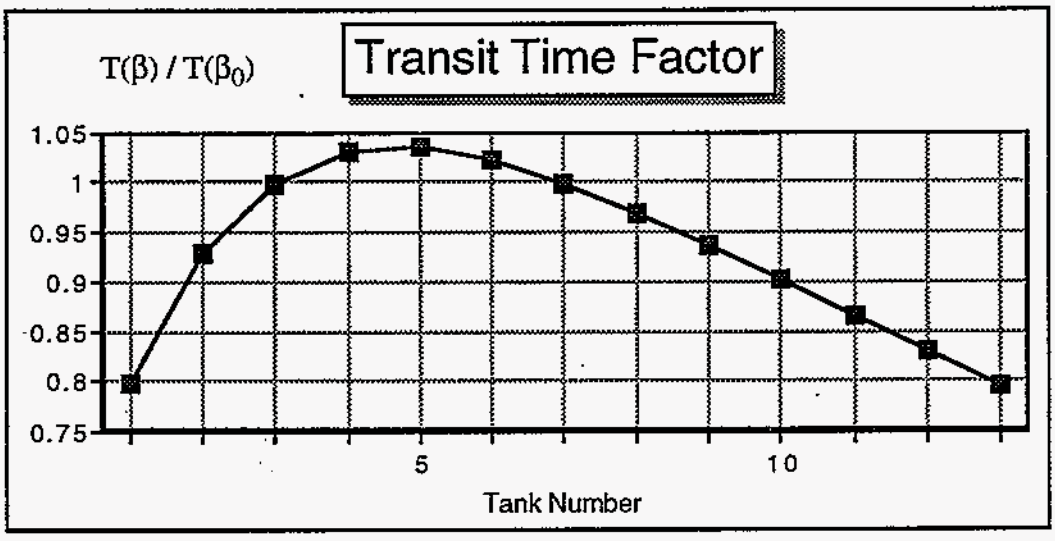

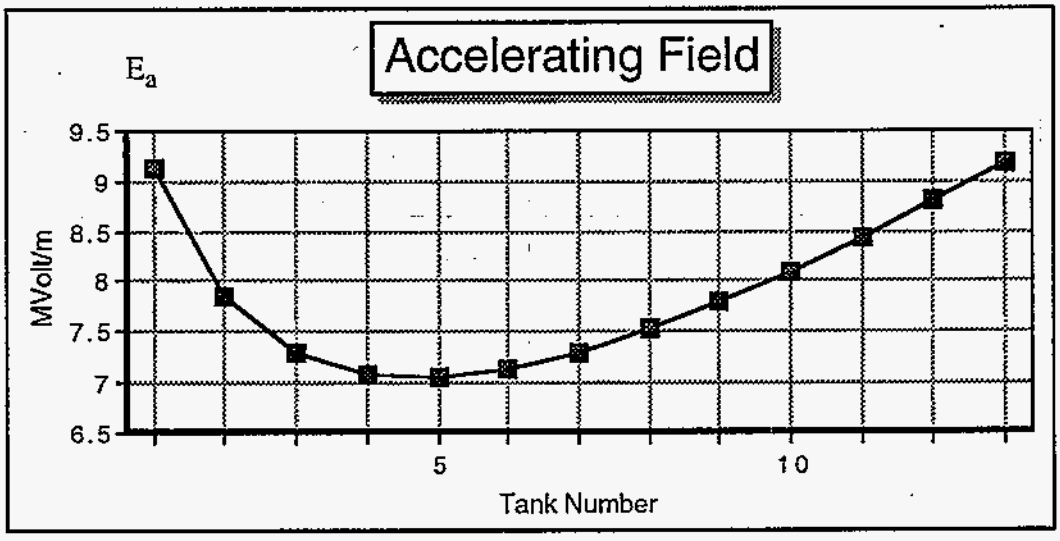

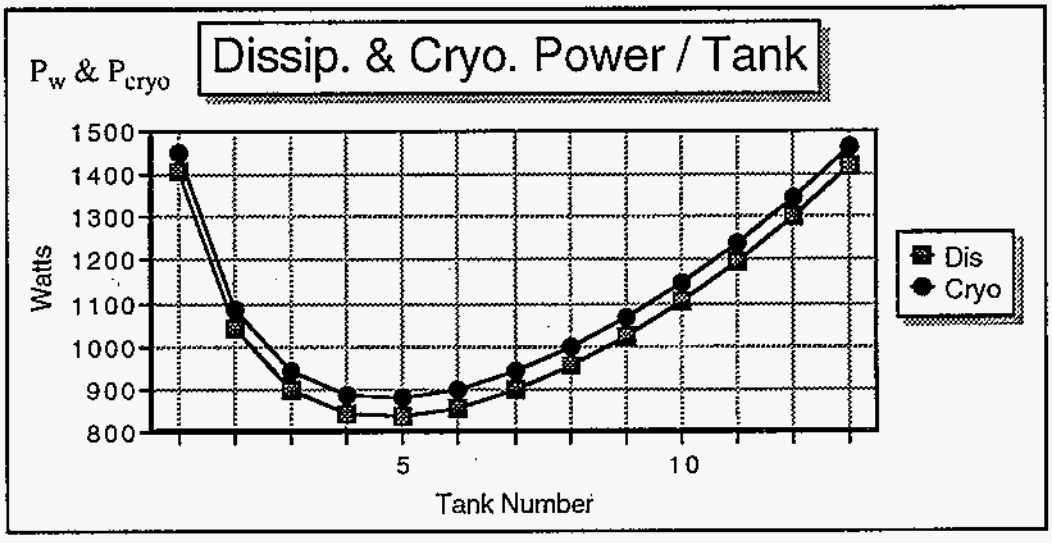

Figure 7. Plots (2) of Behavior versus *period* (tank) number of the Low-Energy Section

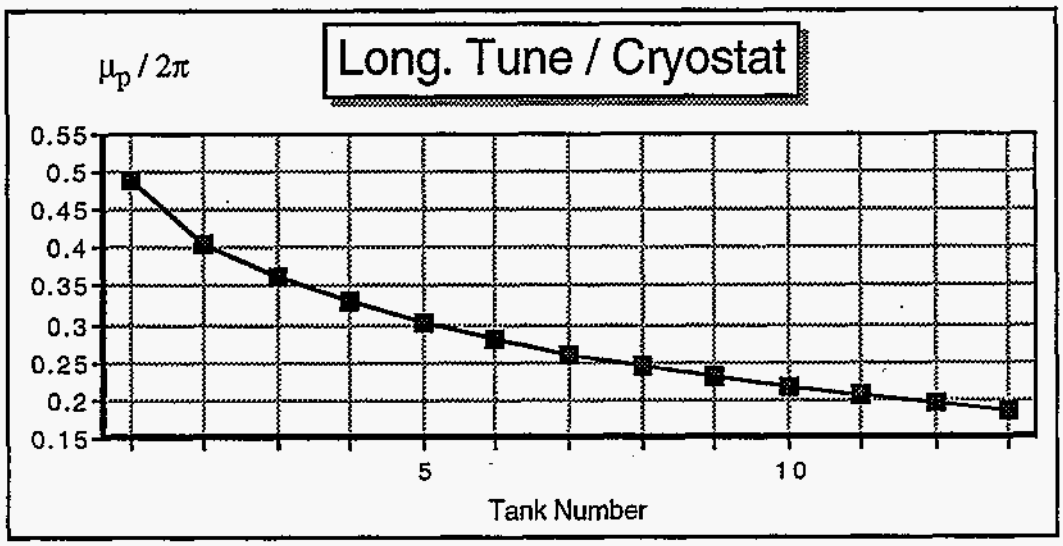

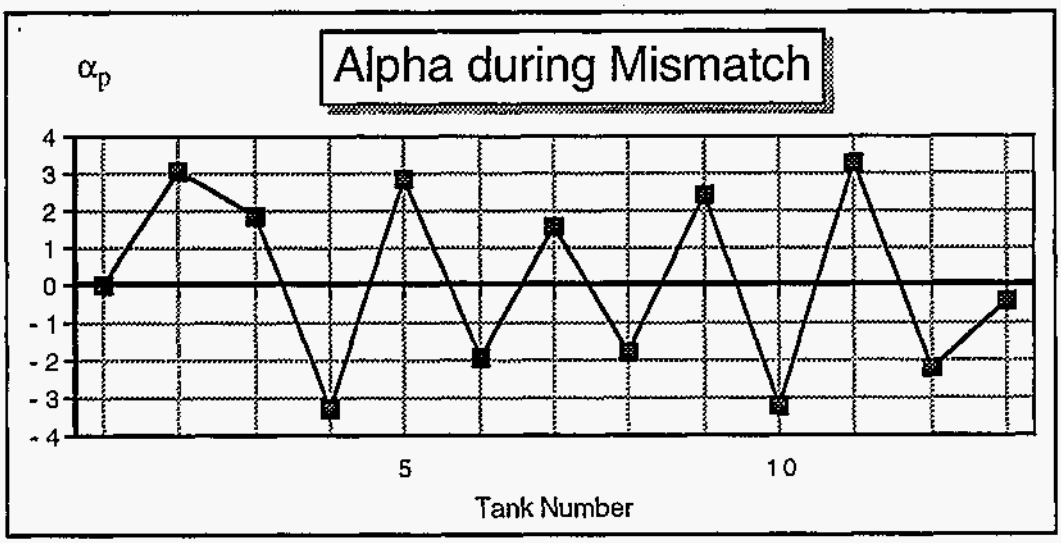

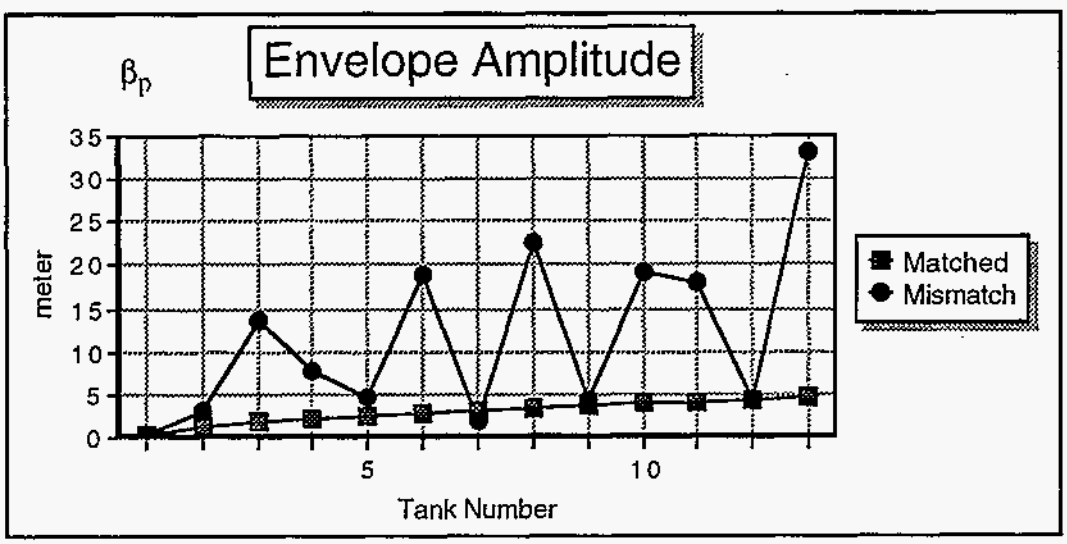

Figure 8. Plots (3) of Behavior versus *period* (tank) number of the Low-Energy Section

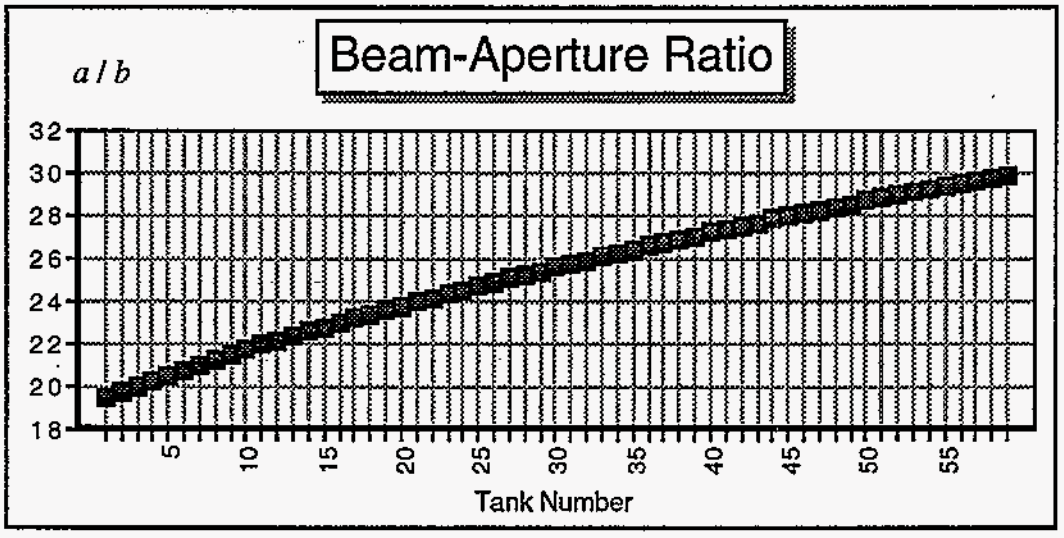

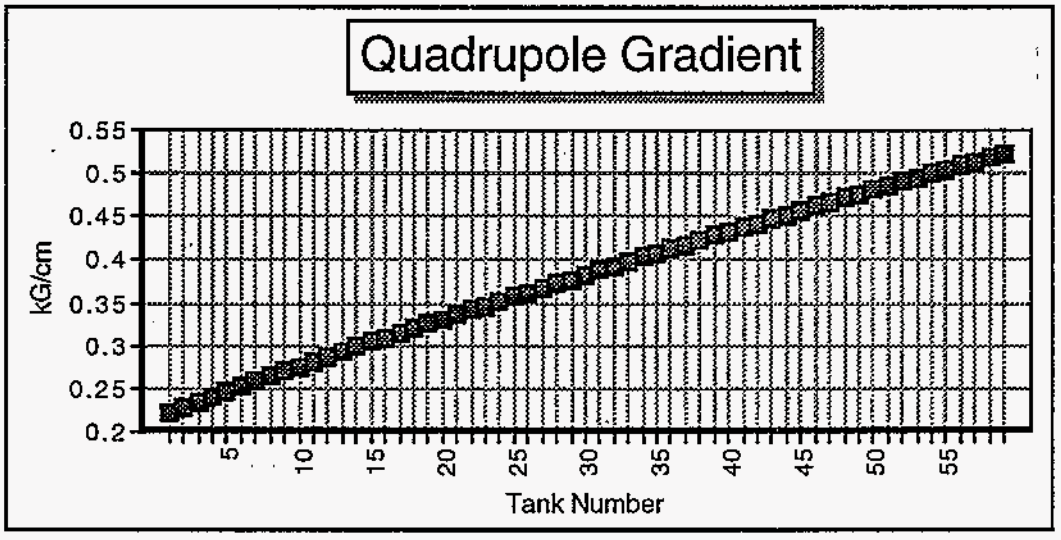

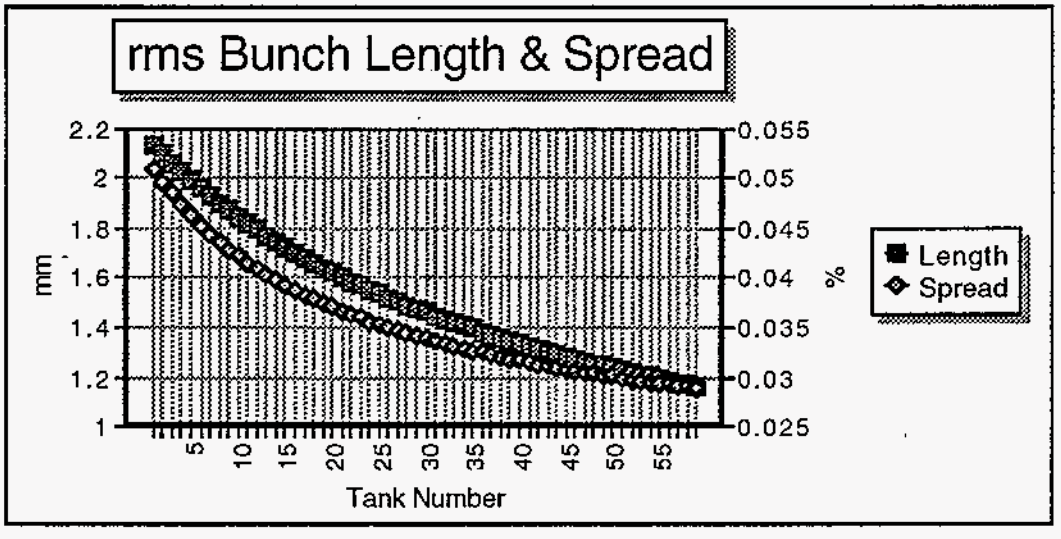

Figure 9. Plots (1) of Behavior versus *period* (tank) number of the Medium-Energy Section

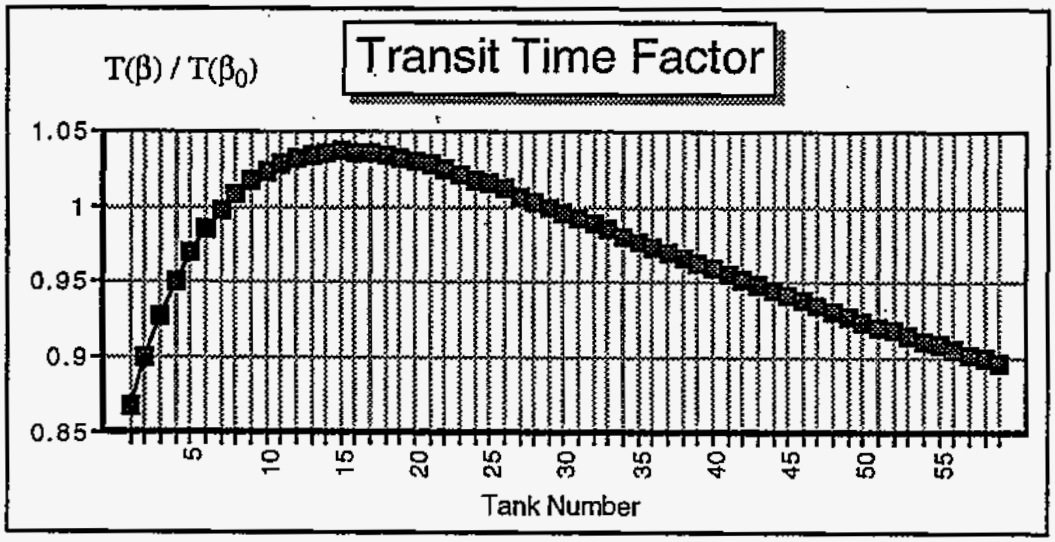

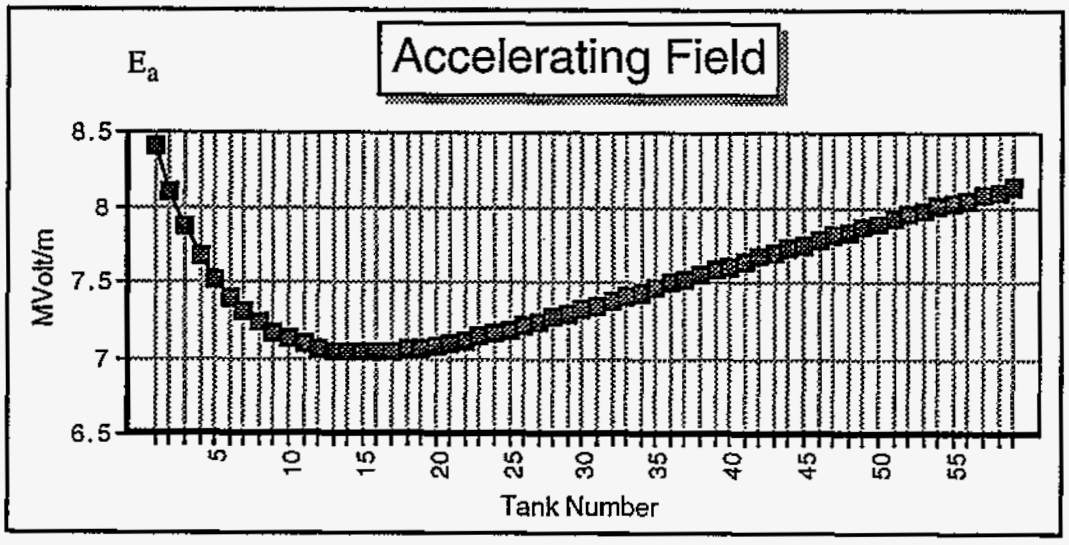

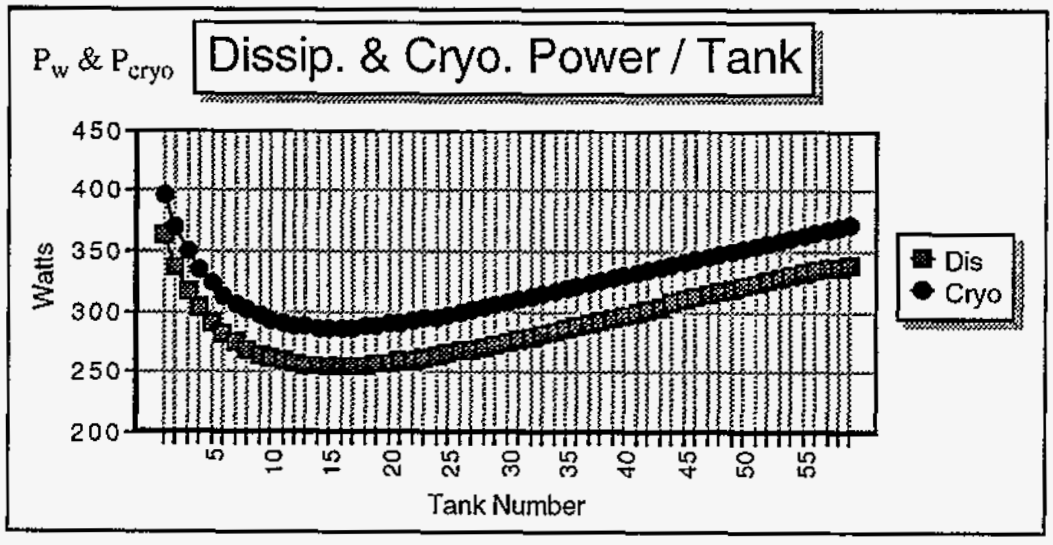

Figure 10. Plots (2) of Behavior versus *period* (tank) number of the Medium-Energy Section

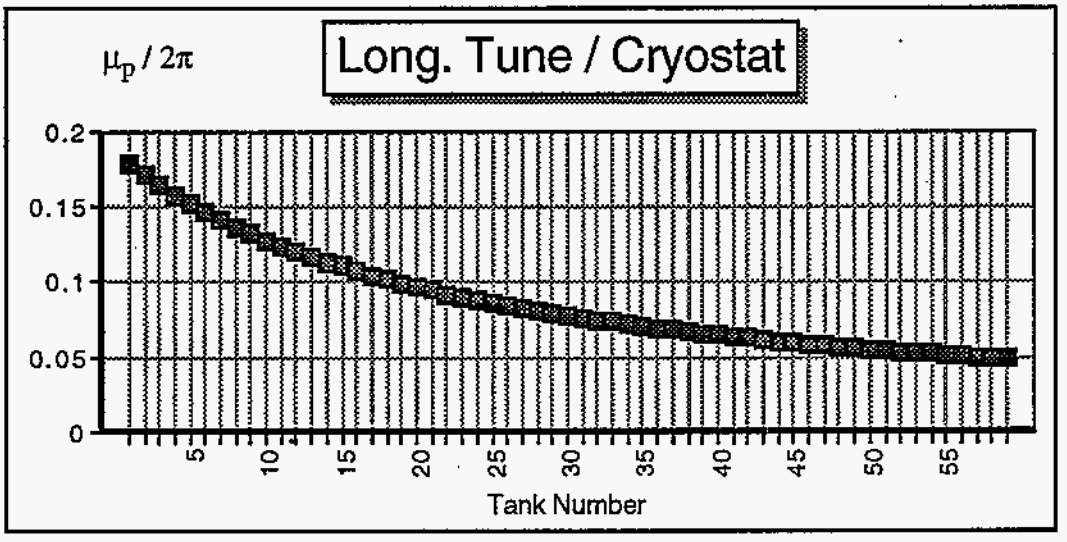

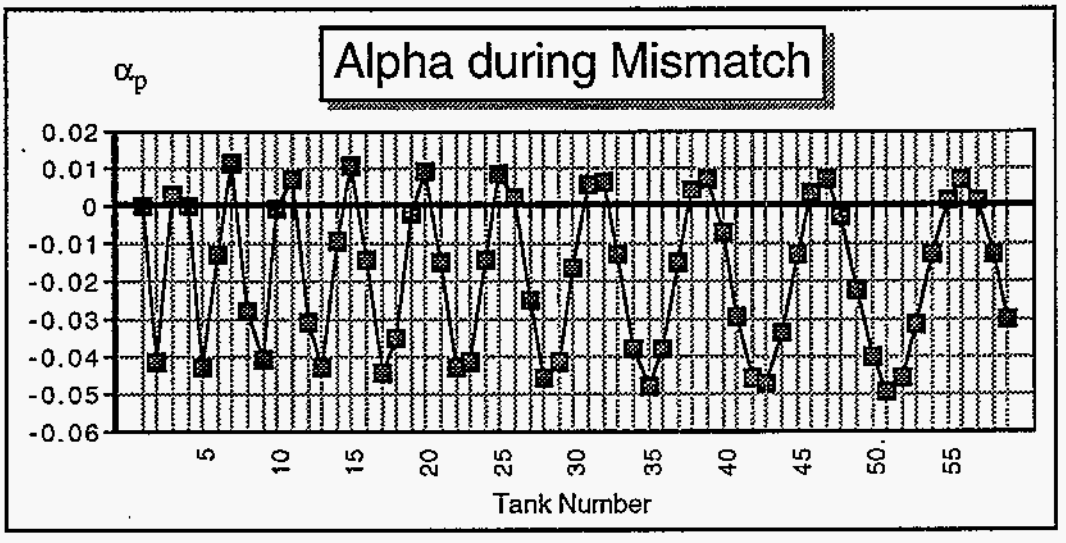

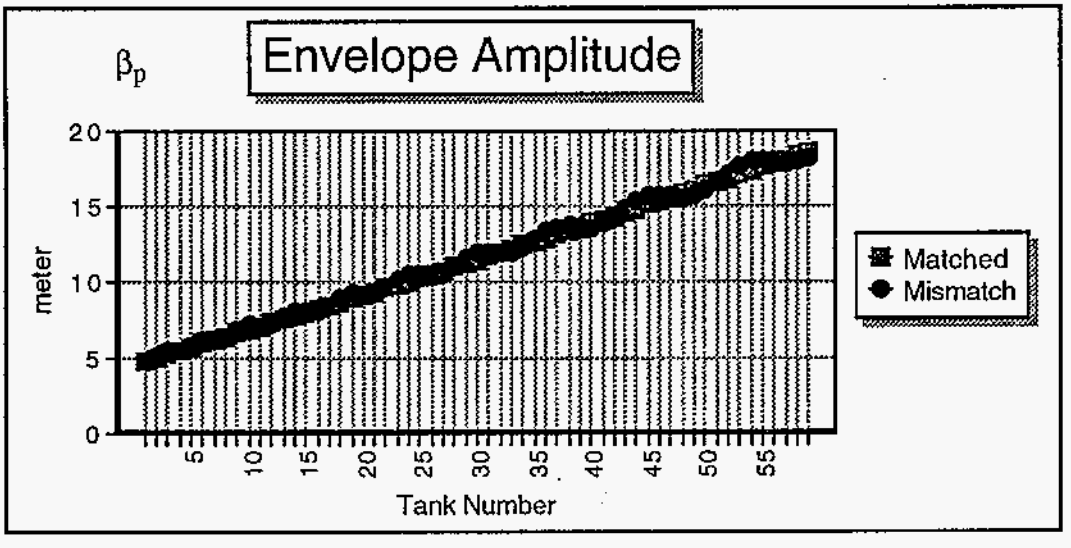

Figure 11. Plots (3) of Behavior versus *period* (tank) number of the Medium-Energy Section

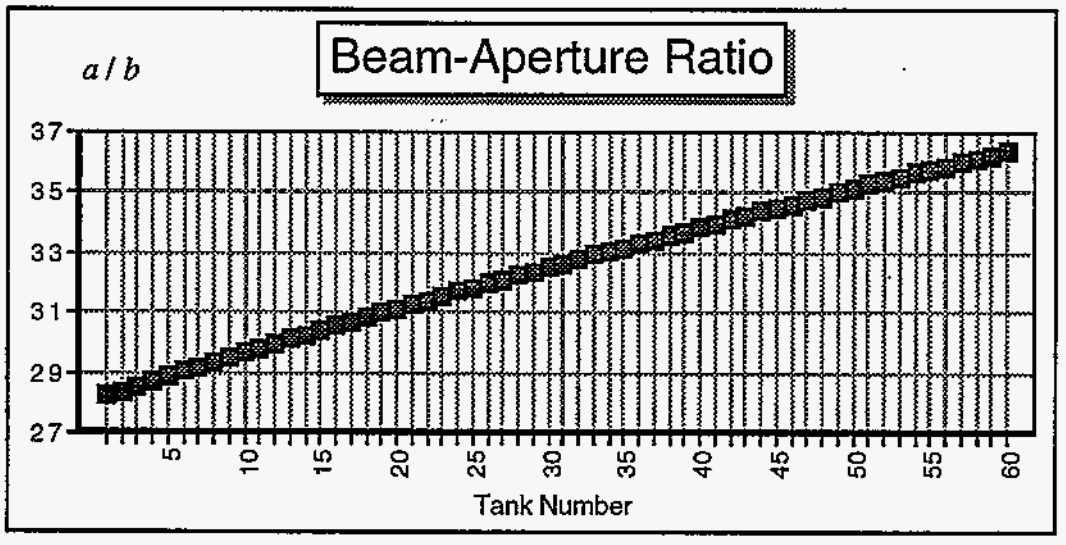

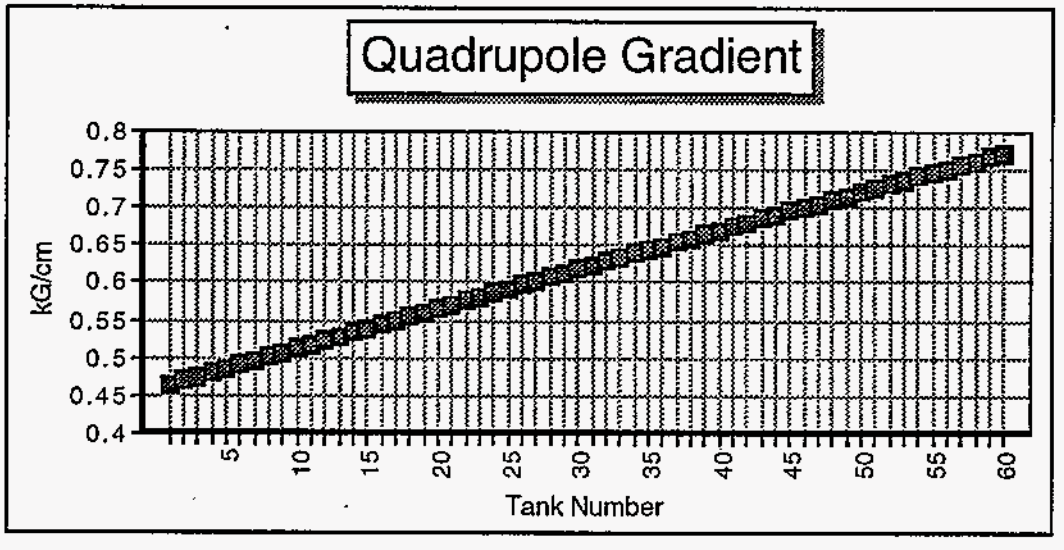

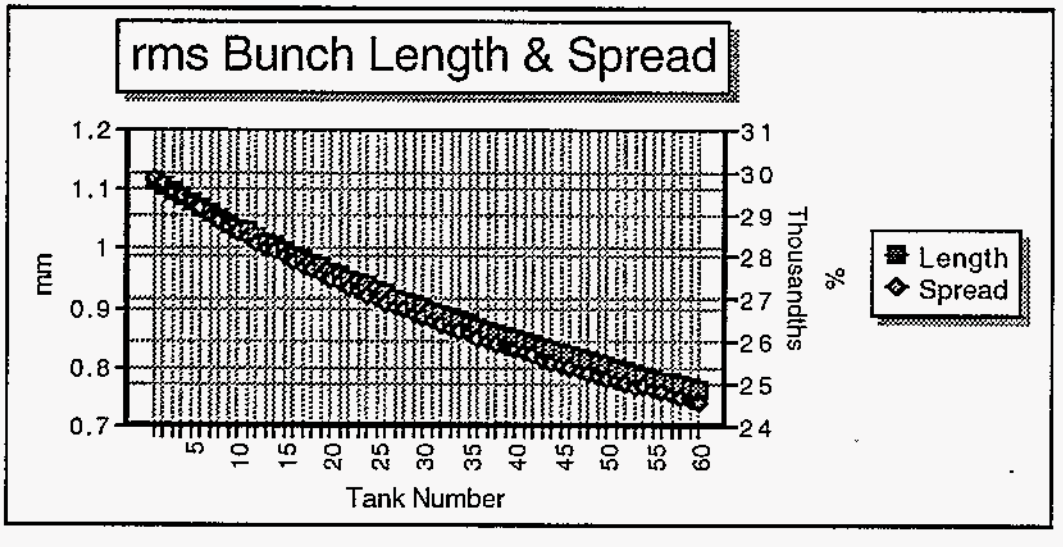

Figure 12. Plots (1) of Behavior versus *period* (tank) number of the High-Energy Section

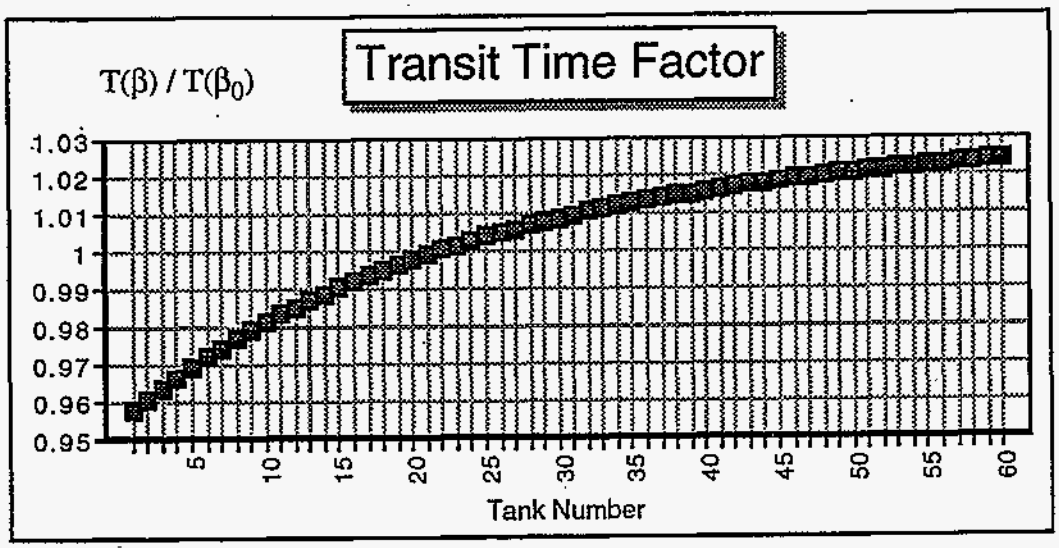

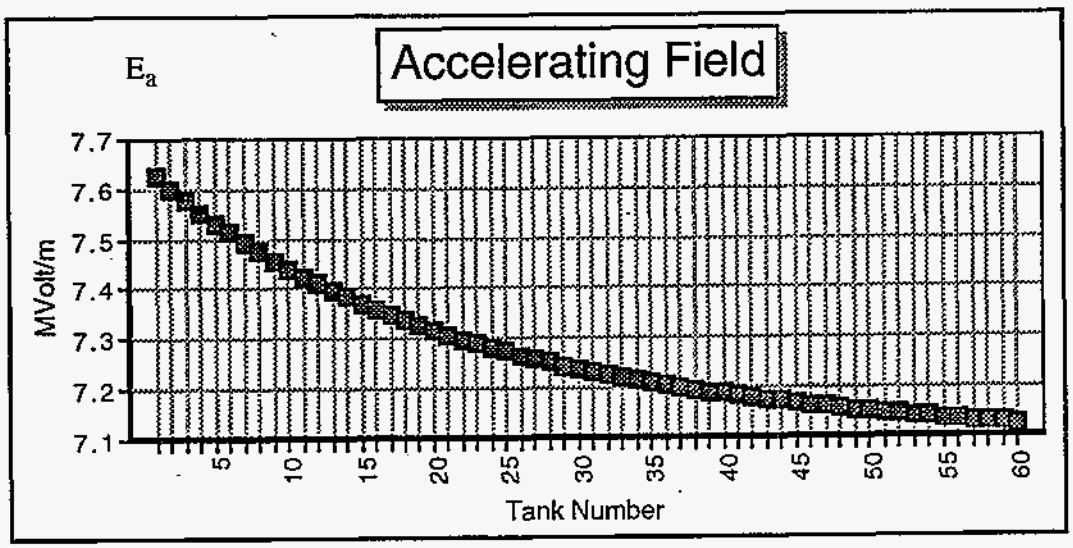

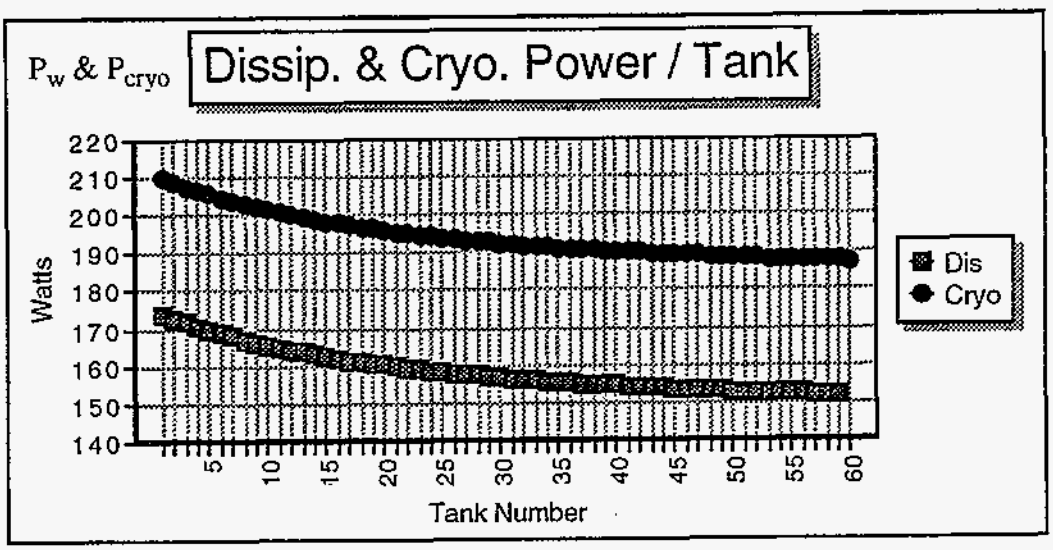

Figure 13. Plots (2) of Behavior versus *period* (tank) number of the High-Energy Section

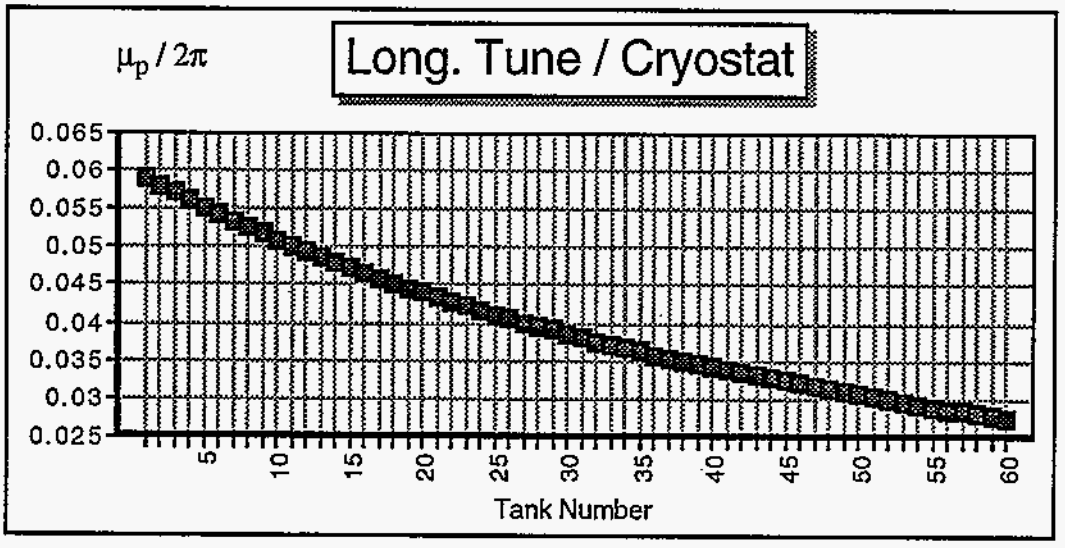

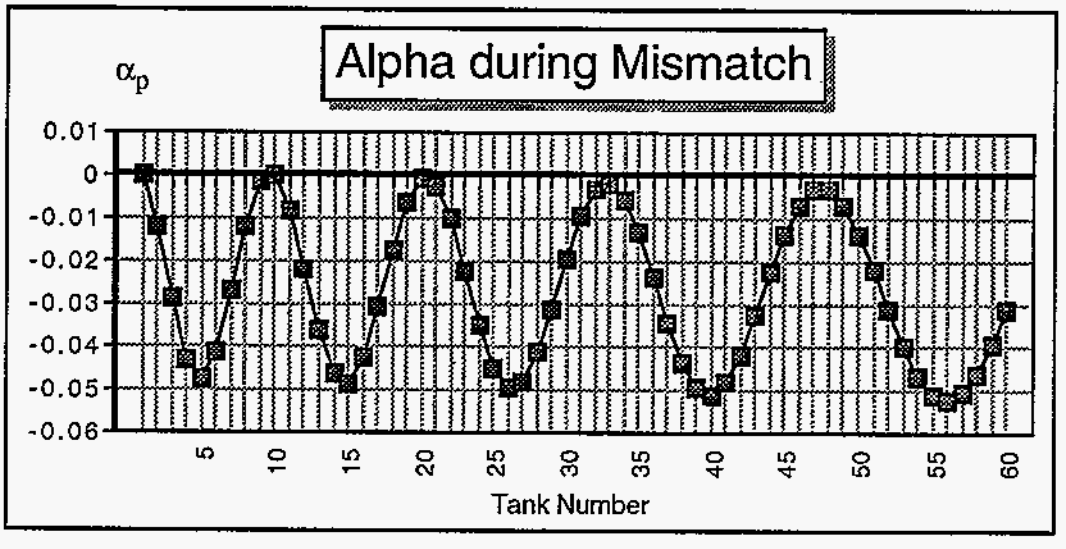

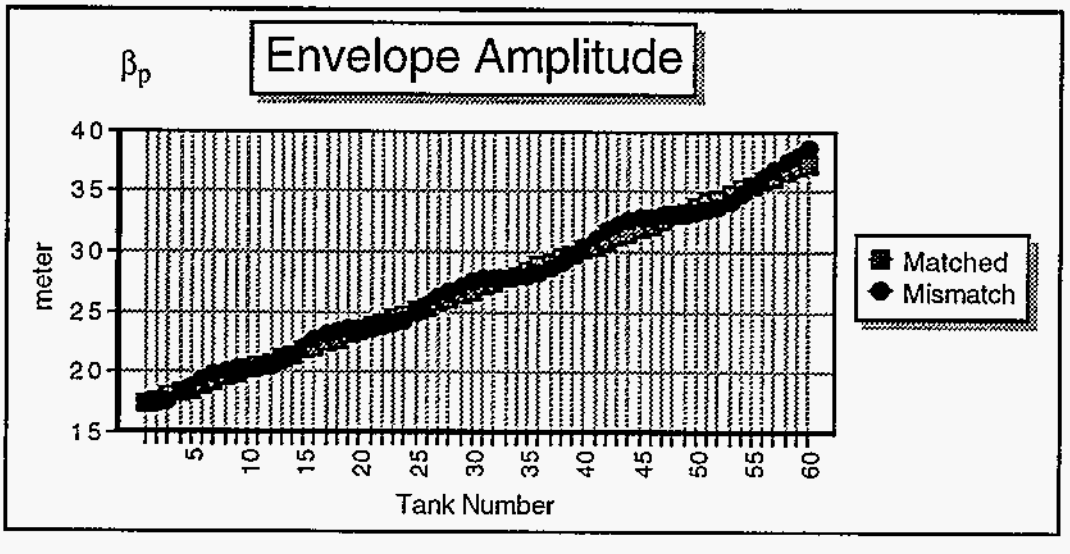

Figure 14. Plots (3) of Behavior versus *period* (tank) number of the High-Energy Section

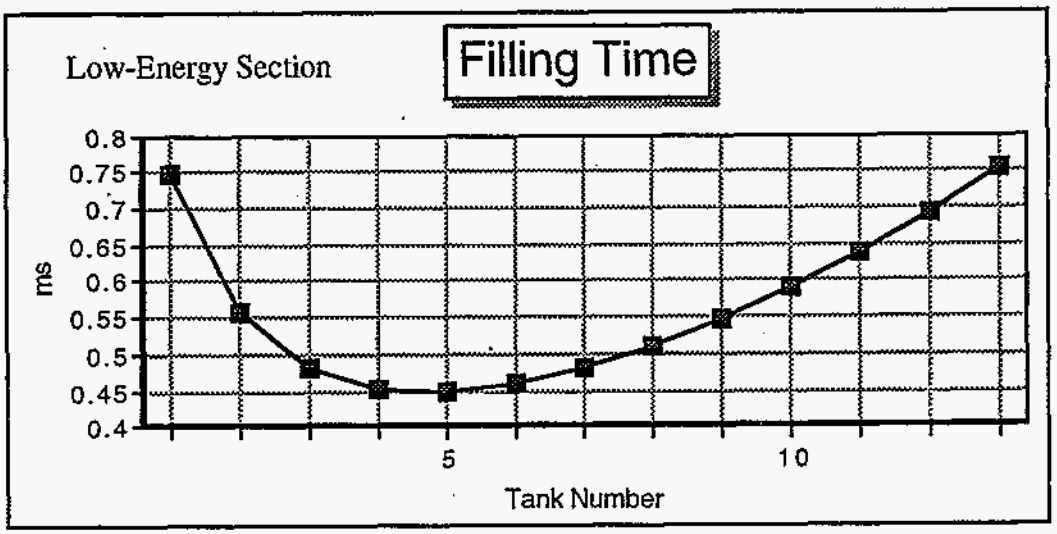

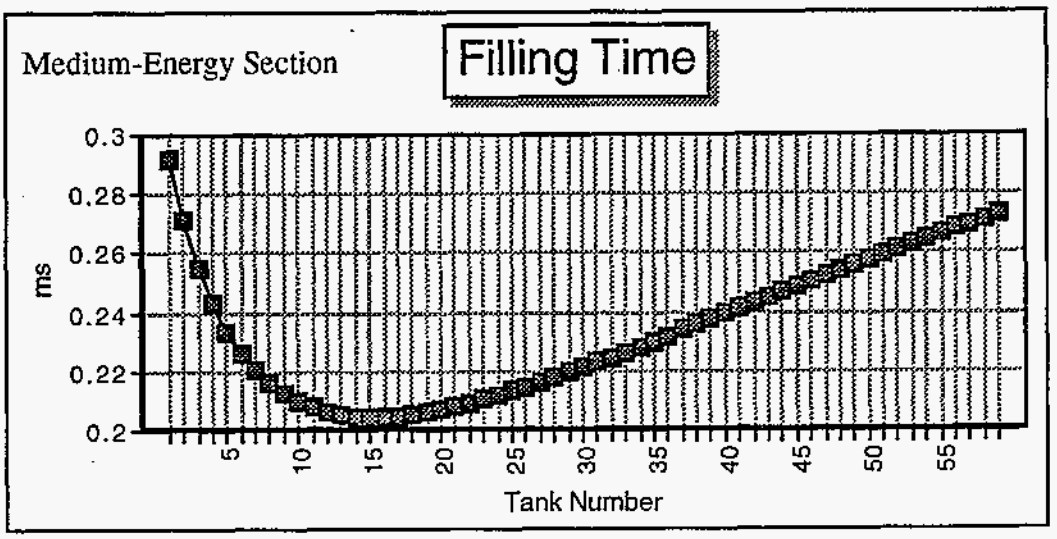

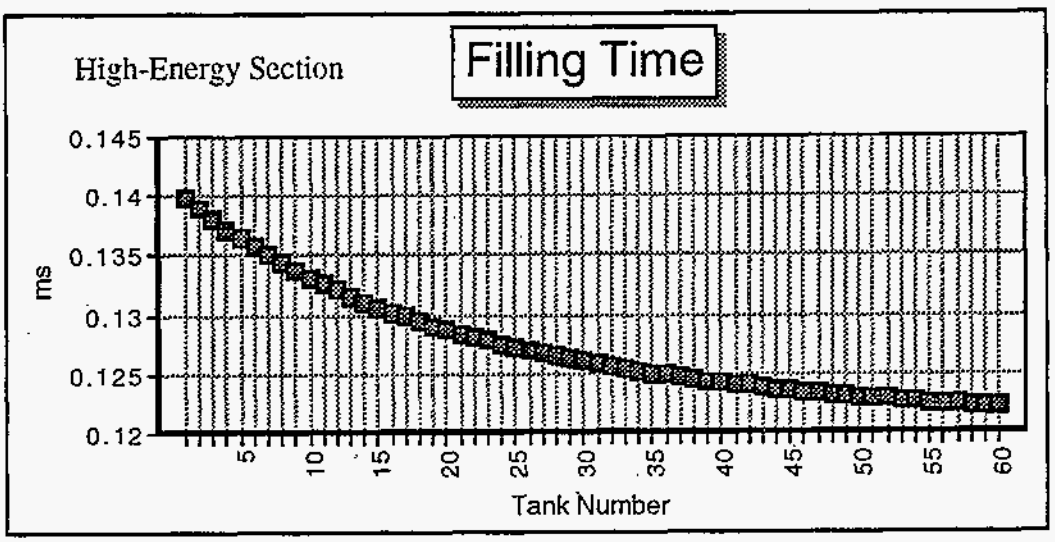

Figure 15. Cavity Filling Time T_f versus *period* (tank) number for the 3 Linac sections

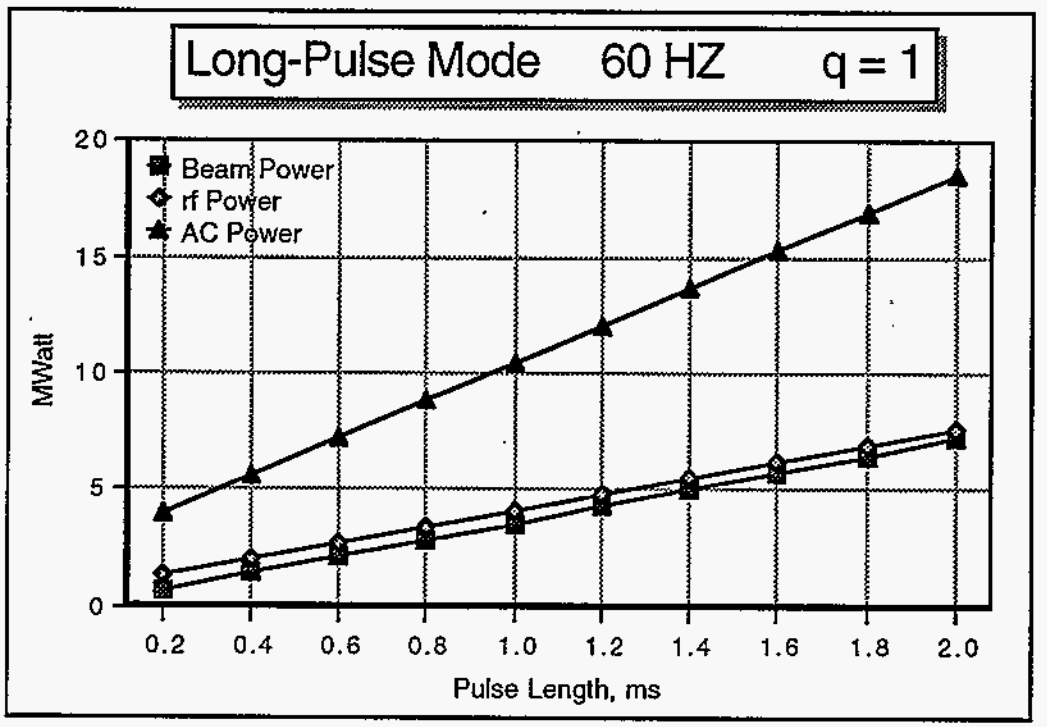

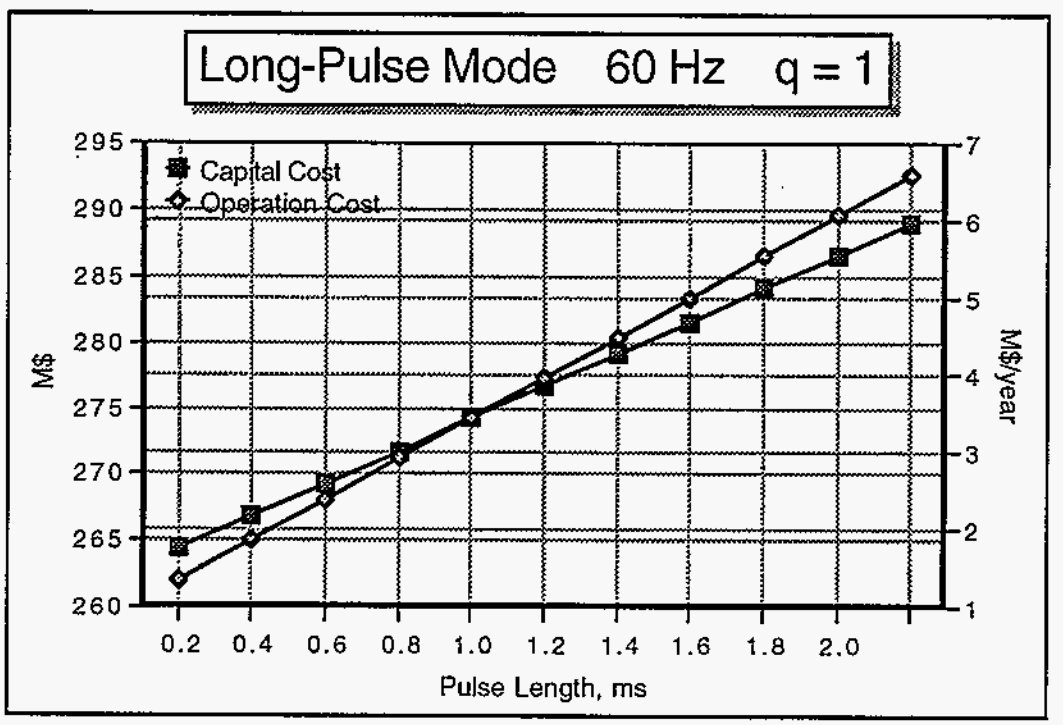

Figure 16. Power and Cost values for the Long-Pulse mode, unchopped, at 60 Hz repetition rate, versus beam Pulse Length T_p

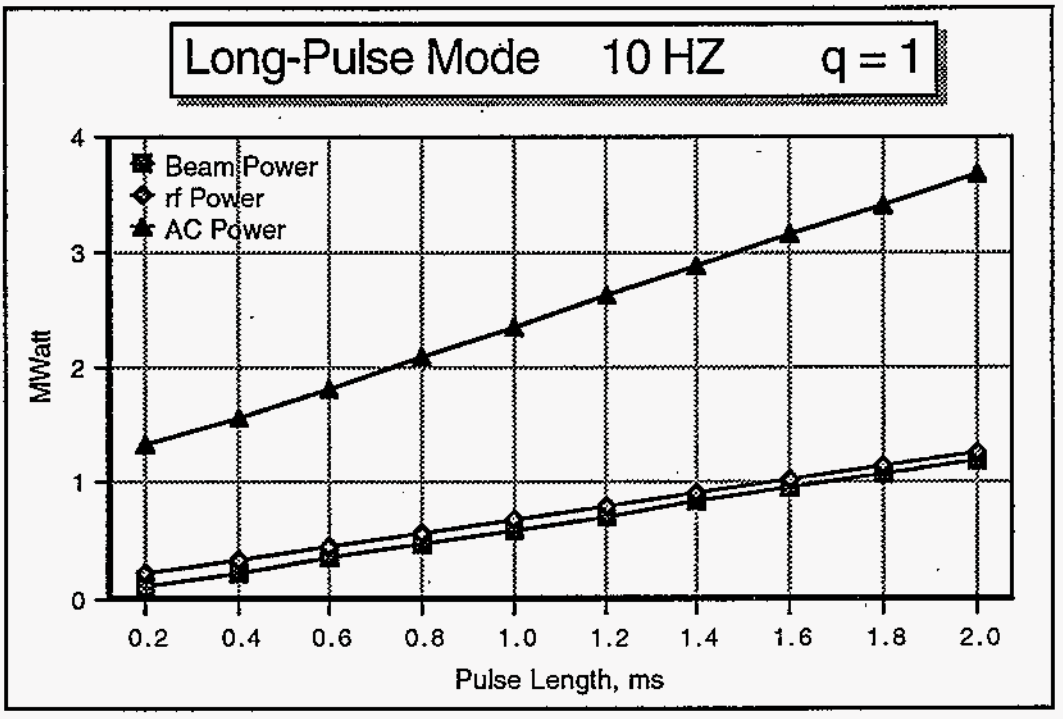

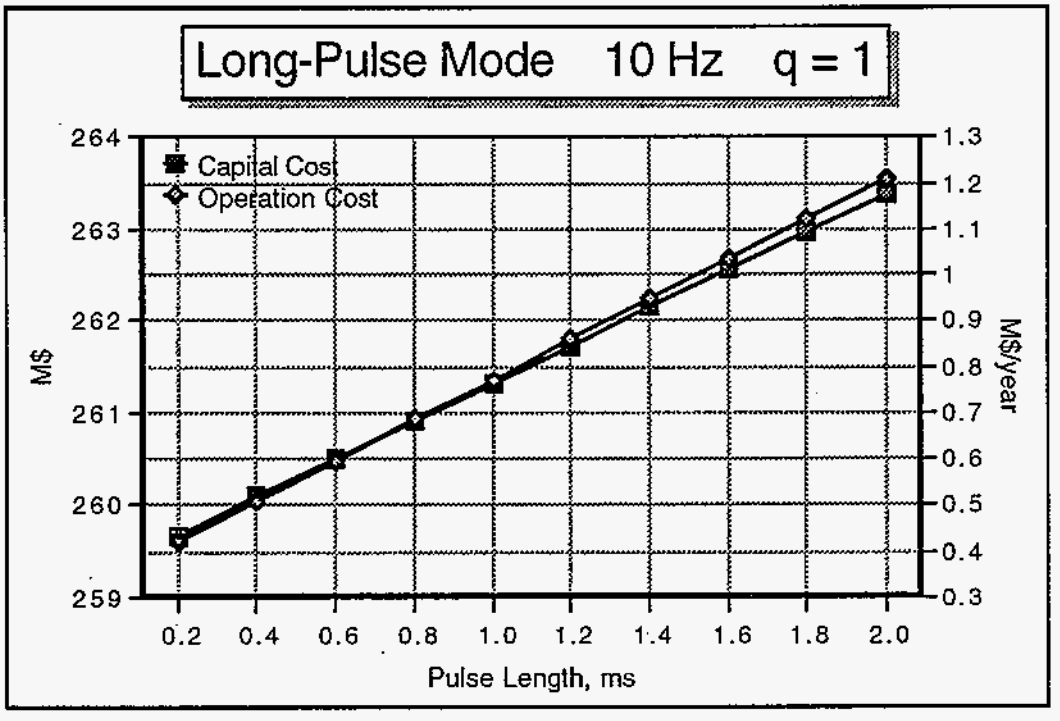

Figure 17. Power and Cost values for the Long-Pulse mode, unchopped, at 10 Hz repetition rate, versus beam Pulse Length T_p